EUROPEAN ORGANIZATION FOR NUCLEAR RESEARCH

CERN-EP-2021-53
01 April 2021

Nuclear modification factor of light neutral-meson spectra up to high transverse momentum in p–Pb collisions at $\sqrt{s_{\mathrm{NN}}}$ = 8.16 TeV

ALICE Collaboration*

August 21, 2022

Abstract

Neutral pion and η meson production cross sections were measured up to unprecedentedly high transverse momenta (p_{T}) in p–Pb collisions at $\sqrt{s_{\mathrm{NN}}} = 8.16$ TeV. The mesons were reconstructed via their two-photon decay channel in the rapidity interval $-1.3 < y < 0.3$ in the ranges of $0.4 < p_{\mathrm{T}} < 200$ GeV/c and $1.0 < p_{\mathrm{T}} < 50$ GeV/c, respectively. The respective nuclear modification factor (R_{pPb}) is presented for p_{T} up to of 200 and 30 GeV/c, where the former was achieved extending the π^0 measurement in pp collisions at $\sqrt{s} = 8$ TeV. The values of R_{pPb} are below unity for $p_{\mathrm{T}} < 10$ GeV/c, while they are consistent with unity for $p_{\mathrm{T}} > 10$ GeV/c. The new data provide constraints for nuclear parton distribution and fragmentation functions over a broad kinematic range and are compared to model predictions as well as previous results at $\sqrt{s_{\mathrm{NN}}} = 5.02$ TeV.

*See Appendix A for the list of collaboration members

1 Introduction

Measurements of identified hadron spectra in high-energy proton–proton (pp) collisions are well suited to constrain perturbative predictions from Quantum Chromodynamics (QCD) [1]. At large momentum transfer (Q^2) one relies in these perturbative QCD (pQCD) calculations on the factorization of computable short-range parton scattering from long-range properties of QCD that need experimental input. These non-perturbative properties are typically modeled by parton distribution functions (PDFs), which describe the fractional-momentum (x) distributions of quarks and gluons within the proton, and fragmentation functions (FFs), which describe the fractional-momentum (z) distribution of quarks or gluons for hadrons of certain species.

In high-energy proton–nucleus (p–A) collisions, nuclear effects are expected to significantly affect particle production, in particular at small x [2]. Previous measurements of neutral pions and charged hadrons in p–Pb collisions at $\sqrt{s_{\mathrm{NN}}} = 5.02$ TeV at the LHC [3–6] indeed revealed distinct deviations from binary-scaled pp collisions, confirming earlier results from deuteron–gold collisions at $\sqrt{s_{\mathrm{NN}}} = 0.2$ TeV at RHIC [7, 8]. The modification at low p_{T} ($\sim$1 GeV/c), which is attributed to nuclear shadowing, can be parameterized by nuclear parton distribution functions (nPDFs) [9, 10]. However, the high parton densities reached at low p_{T} (x as small as $\sim 5\cdot 10^{-4}$) makes the Color Glass Condensate (CGC) framework [11] applicable which predicts strong particle suppression due to saturation of the parton phase space in nuclei [12]. Recently, also parton energy loss in cold nuclear matter was shown [13] to lead to suppressed particle yields at low p_{T}, while at high p_{T} ($\sim$10 GeV/c) parton energy loss in hot nuclear matter may play a role [14].

In this letter, the nuclear modification of particle yields is quantified by

$$R_{\mathrm{pPb}} = \frac{1}{A_{\mathrm{Pb}}} \frac{\mathrm{d}^2\sigma_{\mathrm{pPb}}}{\mathrm{d}p_{\mathrm{T}}\mathrm{d}y} \Bigg/ \frac{\mathrm{d}^2\sigma_{\mathrm{pp}}}{\mathrm{d}p_{\mathrm{T}}\mathrm{d}y}, \tag{1}$$

where $A_{\mathrm{Pb}} = 208$ is the nuclear mass number of lead and $\mathrm{d}^2\sigma/(\mathrm{d}p_{\mathrm{T}}\mathrm{d}y)$ are the π^0 or η meson cross sections measured in p–Pb collisions at $\sqrt{s_{\mathrm{NN}}} = 8.16$ TeV and in the corresponding pp reference system at $\sqrt{s} = 8$ TeV.

2 ALICE detector

The neutral mesons were reconstructed via their two-photon decay channels $\pi^0(\eta) \rightarrow \gamma\gamma$ using different reconstruction techniques provided by the various subdetector systems of ALICE [15, 16]. Photons are either reconstructed using the Electromagnetic Calorimeter (EMCal), the Photon Spectrometer (PHOS) or via the Photon Conversion Method (PCM). The latter uses $\mathrm{e}^+\mathrm{e}^-$ pairs from conversions, which are reconstructed from tracks measured in the Inner Tracking System (ITS) [17] and the Time Projection Chamber (TPC) [17] at $|\eta| < 0.9$ inside a solenoidal magnetic field of $B = 0.5$ T. The EMCal [18, 19] is a lead-scintillator sampling electromagnetic calorimeter at a radial distance of 4.28 m from the interaction point (IP) covering $\Delta\varphi = 100°$ in azimuth for $|\eta| < 0.7$ in pseudorapidity during the 2012 pp data taking period. During the p–Pb data taking in 2016, additional modules [19] were available that extended the coverage to $\Delta\varphi = 107°$ for $|\eta| < 0.7$ and added $\Delta\varphi = 60°$ opposite in azimuth for $0.22 < |\eta| < 0.7$. The calorimeter provides an energy resolution of $\sigma_E/E = 4.8\%/E \oplus 11.3\%/\sqrt{E} \oplus 1.7\%$, with E in units of GeV. In its full configuration, it consists of a total of 18240 cells of transverse size 6×6 cm^2 each. The PHOS [20] is a lead tungstate electromagnetic calorimeter with 12544 channels at a distance of 4.6 m from the IP, covering $\Delta\varphi = 70°$ and $|\eta| < 0.12$. Its high light yield combined with its cell size being only slightly larger than the Molière radius of 2 cm results in an energy resolution of $\sigma_E/E = 1.8\%/E \oplus 3.3\%/\sqrt{E} \oplus 1.1\%$.

3 Data samples and event selection

The p–Pb data at $\sqrt{s_{\mathrm{NN}}} = 8.16$ TeV were recorded in 2016. Due to the equal magnetic rigidity for proton and Pb beams in the LHC, the measurements that were performed in the laboratory system at $|y_{\mathrm{lab}}| < 0.8$, correspond to approximately $-1.3 < y < 0.3$ in the centre-of-mass frame. The minimum bias (MB) event trigger required a coincidence at Level 0 (L0) of signals issued by the V0A and V0C detectors, which are two arrays of 32 scintillator tiles each covering full azimuth at $2.8 < \eta < 5.1$ and $-3.7 < \eta < -1.7$, respectively [21]. Additional triggers at L0 required an energy deposit above 2 GeV for EMCal and 4 GeV for PHOS, in 4×4 adjacent cells in coincidence with the MB trigger. Based on the L0 preselection, further hardware Level 1 triggers were issued, two for the EMCal with energy thresholds at 5.5 GeV and 8 GeV and one for the PHOS at 7 GeV. For the data presented, total integrated luminosities of 11 nb^{-1} for p–Pb and 657 nb^{-1} for pp collisions (recorded in 2012) were inspected.

4 Analysis

Reconstructed tracks were used to determine the primary vertex of the collision, which was required to be within 10 cm from the nominal IP position along the beam direction. Details on event selection, photon and meson reconstruction methods, which are analogous to those described in Refs. [6, 22], are provided in the supplemental material [23]. To achieve an optimal uncertainty cancellation on R_{pPb}, the meson analyses were performed simultaneously for the p–Pb and pp data sets using identical methods and selections, where possible.

Photon reconstruction in the EMCal (PHOS) is based on grouping adjacent cells, with energy deposits above $E_{\mathrm{cell}}^{\mathrm{min}} = 100$ (20) MeV, into clusters starting with a seed cell of $E_{\mathrm{cell}}^{\mathrm{seed}} > 500$ (50) MeV. The thresholds for PHOS are lower due to its better energy resolution and finer granularity. Photon candidates in the EMCal were required to have $|\eta_\gamma| < 0.67$, a minimum of two cells in the cluster ($N_{\mathrm{cell}}^{\mathrm{cls}} \geq 2$), and an elongation ($\sigma^2_{\mathrm{long}}$ [24]) between 0.1 and 0.5. In PHOS, $|\eta_\gamma| < 0.12$ was required and the criteria $\sigma^2_{\mathrm{long}} > 0.1$ and $N_{\mathrm{cell}}^{\mathrm{cls}} \geq 3$ were only applied to clusters with $E > 2$ GeV. Hadron and electron contamination of the photon clusters in the EMCal was removed if an associated track was found with $E/p_{\mathrm{track}} < 1.75$. The E/p veto increased the photon efficiency by up to 50% at high p_{T} with respect to previous measurements [6, 22]. Corrections for the non-linear energy response of the calorimeters were applied to the cluster energy. For the EMCal the correction was obtained from electron test beam data and from laboratory-based measurements of the low-gain shapers in the front-end electronics. The correction is sizeable only at low E (6% at 1 GeV) and at high E (14% at 200 GeV). It includes a residual relative energy-and-position correction, which is applied on simulated EMCal clusters to match the π^0 peak position in data. An improved description of the EMCal cluster properties in simulations was achieved by introducing a cross talk emulation within the same EMCal readout card as described in Ref. [25]. The resulting agreement of the π^0 mass peak position is better than 0.3% between data and simulation. For the PHOS, the energy non-linearity was corrected by fixing the reconstructed π^0 mass to the nominal PDG value [26].

Photon conversions were reconstructed by combining oppositely charged tracks, originating from a common vertex up to a radius of 180 cm, through a secondary vertex finder. Only tracks with a TPC dE/dx within -3σ and $+4\sigma$ of the expected values for electrons were accepted, where σ is the dE/dx resolution. Additionally, tracks with $p > 0.4$ GeV/c and dE/dx up to 1σ above the expected value for pions were rejected. For tracks with $p > 3.5$ GeV/c, this was loosened to 0.5σ. The photon conversion selection criteria were further optimized with respect to previous measurements [22, 27] to yield about 10% better efficiency at similar purity.

An invariant mass ($m_{\gamma\gamma}$) technique was used for the reconstruction of neutral pions and η mesons. For this, $m_{\gamma\gamma}$ was calculated for all possible combinations of photon candidates per event taking either both photons reconstructed by the same method (called PCM, EMC, and PHOS), or one photon reconstructed

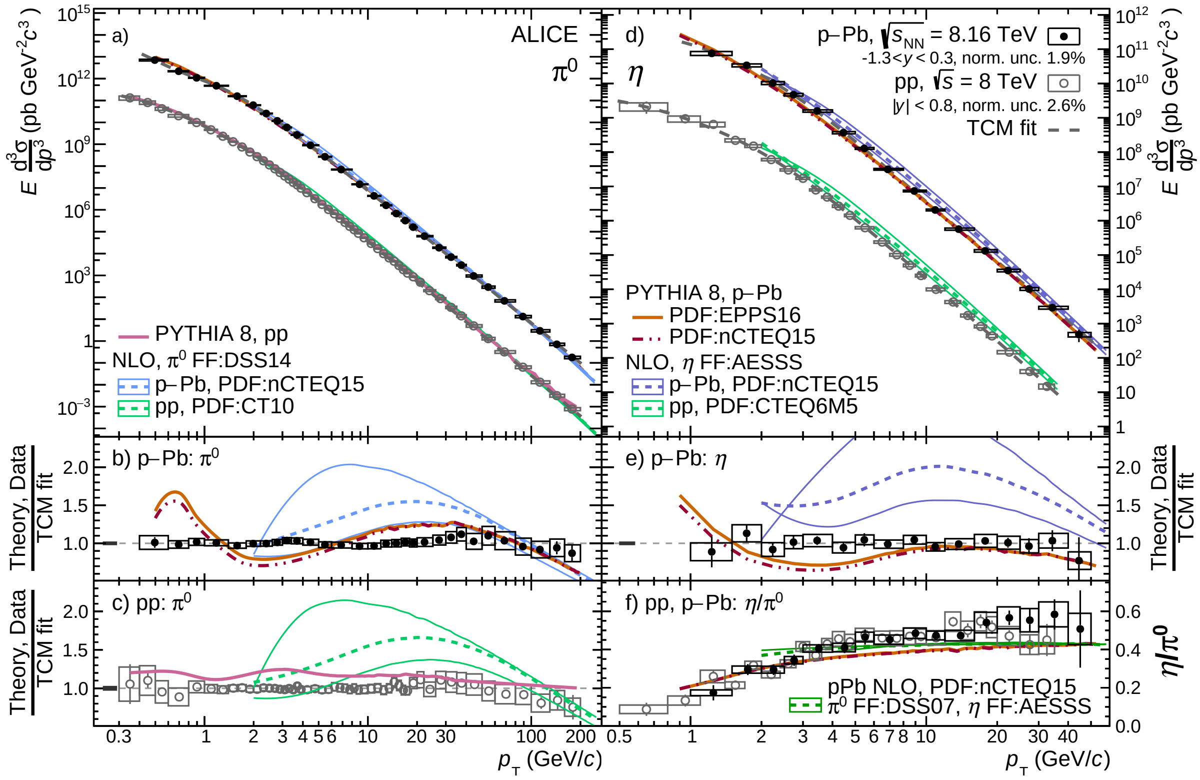

Fig. 1: Neutral pion a) and η meson d) cross sections for pp collisions at $\sqrt{s} = 8$ TeV and p–Pb collisions at $\sqrt{s_{\mathrm{NN}}} = 8.16$ TeV together with TCM fits, NLO calculations [28–31] and PYTHIA 8 [32, 33] predictions using different nPDFs [9, 10]. Statistical uncertainties are shown as vertical bars; the systematic uncertainties as boxes. The ratios of the π^0 spectra in p–Pb and pp collisions to the TCM fits are shown in panel b) and c), respectively, together with the ratios of the calculations to the fits; panel e) shows the same for η mesons in p–Pb collisions. In panel f) the η/π^0 ratios in pp and p–Pb collisions are compared to theory predictions. The normalization uncertainty in the spectra ratio panels is indicated as a solid gray box around unity.

with PCM and one with EMC (called PCM-EMC). The invariant mass distributions were calculated in p_{T} intervals of the meson candidates (examples are shown in Ref. [23]). For each interval, the combinatorial background, obtained from event mixing, and residual correlated background were subtracted (see Ref. [23]). The remaining distributions were then integrated in $\sim 3\sigma$ around the fitted mass peak position to determine the raw yields.

Neutral pions with $p_{\mathrm{T}} > 16$ GeV/c were measured with the merged-cluster (mEMC) method [27], which exploits single clusters in the EMCal that result from overlapping energy deposits of both decay photons in the same cluster due to the small opening angle for large pion momentum. The elongation ($\sigma^2_{\mathrm{long}} > 0.27$) of clusters with $p_{\mathrm{T}} > 16$ GeV/c was used to discriminate between single-photon ($\sigma^2_{\mathrm{long}} \approx 0.25$) and merged-photon clusters. The σ^2_{long} distribution was obtained in p_{T}-intervals of the clusters (examples are shown in [23]), and the integrated counts above 0.27 were used as raw π^0 candidate yields. The resulting π^0 purity is between 81–87% decreasing with p_{T} in p–Pb and 83–89% in pp collisions. It was determined via PYTHIA 8 [32] simulations with additional data-driven corrections, which increase the relative fractions of prompt photons by 1–3% and of η mesons by 2%. POWHEG-Box [34, 35] simulations were used to determine an additional purity correction for electrons from weak decays of up to 3%.

Correction factors for reconstruction efficiency and kinematic acceptance (see Ref. [23]) were obtained from simulations of the detector response with GEANT3 [36] using DPMJET [37] and PYTHIA 8 [32] as event generators. The correction factors for secondary π^0 from long-lived strange hadron decays were obtained from a particle-decay simulation based on measured spectra and are dominated by contributions from $\mathrm{K}^0_{\mathrm{S}}$ and Λ decays [22, 38]. They amount to about 1–6% and decrease with p_{T}. For the PCM method, an additional correction for out-of-bunch pileup of 7 to 15% decreasing with p_{T} was applied.

The spectra were normalized by the integrated luminosities of each trigger sample and meson reconstruction method as explained in Refs. [23] and [22].

The systematic uncertainties on the π^0 (η) cross sections contain contributions from the yield extraction of 1–10% (2–20%) depending on the reconstruction method and p_{T}. Further contributions from the imperfect description of the selection variables in the simulation amount to 1–4% (1–6%), while the p_{T}-independent material-budget uncertainties are 4.5% per PCM photon, 2.8% per EMCal photon and 2% per PHOS photon. Uncertainties arising from the out-of-bunch pileup determination reach 3–5% and global uncertainties on the trigger rejection factors are 2–3% [23]. For the mEMC analysis, the largest systematic uncertainty arises from the shower overlaps in jets, which depend on the jet fragmentation and affect the π^0 energy resolution in the EMCal. This uncertainty was estimated as 7–10%, obtained from varying the particle overlaps within clusters. The total uncertainties on the $\pi^0(\eta)$ cross sections are between 5(8)% and 20(27)% and, due to uncertainty cancellations and correlations, between 7% and 24% on the η/π^0 ratio. For the R_{pPb}, the p_{T}-independent uncertainties cancel as well as a fraction of the remaining uncertainties resulting in a total uncertainty between 4(11)% and 25(32)%.

5 Results

The invariant differential cross sections and R_{pPb} measured by each method are consistent within their uncertainties (see [23]). For the calculation of R_{pPb} the spectra are shifted in the y-direction, while for the cross sections they are shifted along the p_{T}-axis to account for the finite bin width [39]. They were combined using the Best Linear Unbiased Estimate (BLUE) method [40, 41] accounting for the partially correlated uncertainties. The resulting π^0 and η invariant differential cross sections for p–Pb collisions at $\sqrt{s_{\mathrm{NN}}} = 8.16$ TeV are shown in Fig. 1 together with the π^0 cross section in pp collisions at $\sqrt{s} = 8$ TeV. This measurement reaches $p_{\mathrm{T}} = 200$ GeV/c, superseding the previous pp measurement that reached 35 GeV/c [22]. The data is compared to a two-component model (TCM) fit [42], NLO calculations [28–31], and PYTHIA 8 [32, 33] predictions using different nPDFs [9, 10]. NLO calculations using the CT10 [43] or CTEQ6M5 [31] PDFs and nCTEQ15 [9] nPDF together with DSS14 [29] or AESSS [30] fragmentation functions generally overestimate the π^0 and η spectra, while predicting a steeper falling spectrum at high p_{T}. In Fig. 1 they are shown with factorization and renormalization scales varied from $\mu = p_{\mathrm{T}}$ to $\mu = 0.5 p_{\mathrm{T}}$ and $2 p_{\mathrm{T}}$ and indicated by bands. PYTHIA 8 [32] calculations using EPPS16 [10] and nCTEQ15 [9] nPDFs describe the data, however without fully capturing the shape of the π^0 spectra, in particular at low and intermediate p_{T}, and with a tendency to underestimate the η spectra. For the η/π^0 ratio, presented in Fig. 1f, the differences in the shape and scale between data and calculations approximately cancel. The ratio is rather well described by the predictions and is consistent over the full p_{T} range between both collision systems. For $p_{\mathrm{T}} > 4$ GeV/c, the η/π^0 ratio is $C^{\eta/\pi^0}_{\mathrm{pPb}} = 0.479 \pm 0.009(\mathrm{stat}) \pm 0.010(\mathrm{syst})$, consistent with the previous measurement at a lower centre-of-mass energy [6] and with $C^{\eta/\pi^0}_{\mathrm{pp}} = 0.473 \pm 0.006(\mathrm{stat}) \pm 0.011(\mathrm{syst})$, the reevaluated η/π^0 ratio in pp collisions at 8 TeV.

To provide the pp reference for the R_{pPb}, the pp spectra measured at $\sqrt{s} = 8$ TeV were scaled to the p–Pb collision energy and corrected for the rapidity difference, using the ratio of π^0 spectra generated with PYTHIA 8 Monash 2013 [33] for both kinematic regions, leading to a 1–2% increase over the whole p_{T} range. The resulting R_{pPb} at $\sqrt{s_{\mathrm{NN}}} = 8.16$ TeV is shown in Fig. 2a for both mesons together with theory predictions and in Fig. 2b compared to data taken at $\sqrt{s_{\mathrm{NN}}} = 5.02$ TeV. In the intermediate p_{T} region, the charged particle R_{pPb} exhibits an enhancement compared to the π^0 data, which is historically attributed to the stronger Cronin effect for baryons [44, 45]. For $p_{\mathrm{T}} > 10$ GeV/c, no deviation from unity is observed within uncertainties for both mesons, consistent with predictions and the ALICE π^0 and $h^{\pm}$ measurements at $\sqrt{s_{NN}} = 5.02$ TeV [6, 46], in contrast to the moderate enhancement for charged hadrons seen by the CMS experiment [5]. Fitting with a constant function resulted in 1.00 ± 0.01 (0.96 ± 0.04) with a χ^2/NDF of 1.04 (0.45) for the π^0 (η) meson. The data do not rule out a possible few-percent contribution from final-state effects in the region between 10 and 20 GeV/c for both mesons [47].

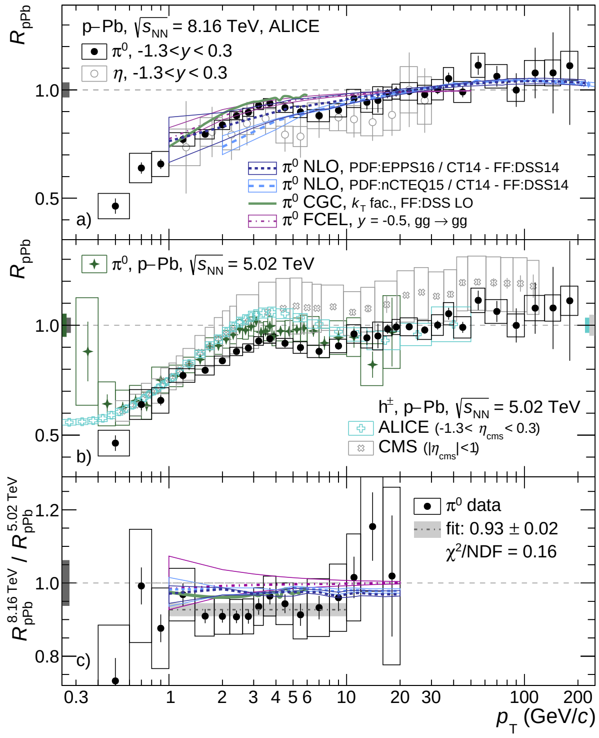

Fig. 2: a) R_{pPb} for π^0 and η mesons in p–Pb collisions at $\sqrt{s_{NN}} = 8.16$ TeV together with NLO [9, 10], CGC [12] and FCEL [13] predictions. b) R_{pPb} for π^0 at $\sqrt{s_{NN}} = 8.16$ TeV compared with π^0 [6] and charged hadron measurements [5, 46] at $\sqrt{s_{NN}} = 5.02$ TeV. c) Ratio of the π^0 R_{pPb} at $\sqrt{s_{NN}} = 8.16$ TeV to that at $\sqrt{s_{NN}} = 5.02$ TeV together with corresponding CGC and FCEL model predictions. Statistical uncertainties are shown as vertical bars; the systematic uncertainties as boxes. The overall normalization uncertainties are indicated as solid boxes around unity and amount to 3.4% in a) and b), and to 6.2% in c).

For $p_T < 10$ GeV/c, a suppression of similar magnitude is observed for both mesons within uncertainties. The suppression is described by NLO calculations using EPPS16 [10] and nCETQ15 [9] nPDFs (the latter tends to underpredict the data below 5 GeV/c), as well as by models using gluon recombination as the CGC-based calculations [12] or parton energy loss in cold nuclear matter in the framework of fully coherent energy loss (FCEL) [13].

The comparison of the π^0 R_{pPb} to the previous measurement at $\sqrt{s_{NN}} = 5.02$ TeV [6], as shown in Fig. 2c, is consistent with unity within uncertainties, but the data hints at a stronger suppression with increasing centre-of-mass energy. A stronger suppression could originate from larger shadowing in the nPDFs, which due to the smaller x probed at 8.16 TeV predict a ratio of about 0.98 in the low p_T region, or from the increasing relevance of gluon saturation, as indicated by the CGC calculation [12]. The FCEL calculation predicts a negligible difference between the two collision energies excluding coherent energy loss as the cause of a stronger suppression. A constant fit for $p_T < 10$ GeV/c yields a ratio of $0.93 \pm 0.02_{tot} \pm 0.06_{norm}$, where the normalization uncertainty is dominated by the interpolation of the π^0 reference spectrum at 5.02 TeV. Further insight may be gained with a measured pp reference at $\sqrt{s} = 5.02$ TeV to reduce uncertainties.

6 Summary

In summary, cross sections for π^0 and η mesons in p–Pb collisions at $\sqrt{s_{\mathrm{NN}}} = 8.16$ TeV were measured for $0.4 < p_{\mathrm{T}} < 200$ GeV/c and $1.0 < p_{\mathrm{T}} < 50$ GeV/c, respectively, providing constraints for nuclear parton distributions and fragmentation functions over an unprecedented kinematic range for light mesons. By extending the reference π^0 measurement in pp collisions at $\sqrt{s} = 8$ TeV to the same p_{T} range using the mEMC method, the R_{pPb} for π^0 was measured up to 200 GeV/c. The R_{pPb} measurement is consistent with unity above 10 GeV/c and shows a suppression at low p_{T}, consistent with theory predictions that also include gluon shadowing or saturation effects.

Acknowledgements

The ALICE Collaboration would like to thank all its engineers and technicians for their invaluable contributions to the construction of the experiment and the CERN accelerator teams for the outstanding performance of the LHC complex. The ALICE Collaboration gratefully acknowledges the resources and support provided by all Grid centres and the Worldwide LHC Computing Grid (WLCG) collaboration. The ALICE Collaboration acknowledges the following funding agencies for their support in building and running the ALICE detector: A. I. Alikhanyan National Science Laboratory (Yerevan Physics Institute) Foundation (ANSL), State Committee of Science and World Federation of Scientists (WFS), Armenia; Austrian Academy of Sciences, Austrian Science Fund (FWF): [M 2467-N36] and Nationalstiftung für Forschung, Technologie und Entwicklung, Austria; Ministry of Communications and High Technologies, National Nuclear Research Center, Azerbaijan; Conselho Nacional de Desenvolvimento Científico e Tecnológico (CNPq), Financiadora de Estudos e Projetos (Finep), Fundação de Amparo à Pesquisa do Estado de São Paulo (FAPESP) and Universidade Federal do Rio Grande do Sul (UFRGS), Brazil; Ministry of Education of China (MOEC) , Ministry of Science & Technology of China (MSTC) and National Natural Science Foundation of China (NSFC), China; Ministry of Science and Education and Croatian Science Foundation, Croatia; Centro de Aplicaciones Tecnológicas y Desarrollo Nuclear (CEADEN), Cubaenergía, Cuba; Ministry of Education, Youth and Sports of the Czech Republic, Czech Republic; The Danish Council for Independent Research | Natural Sciences, the VILLUM FONDEN and Danish National Research Foundation (DNRF), Denmark; Helsinki Institute of Physics (HIP), Finland; Commissariat à l'Energie Atomique (CEA) and Institut National de Physique Nucléaire et de Physique des Particules (IN2P3) and Centre National de la Recherche Scientifique (CNRS), France; Bundesministerium für Bildung und Forschung (BMBF) and GSI Helmholtzzentrum für Schwerionenforschung GmbH, Germany; General Secretariat for Research and Technology, Ministry of Education, Research and Religions, Greece; National Research, Development and Innovation Office, Hungary; Department of Atomic Energy Government of India (DAE), Department of Science and Technology, Government of India (DST), University Grants Commission, Government of India (UGC) and Council of Scientific and Industrial Research (CSIR), India; Indonesian Institute of Science, Indonesia; Istituto Nazionale di Fisica Nucleare (INFN), Italy; Institute for Innovative Science and Technology , Nagasaki Institute of Applied Science (IIST), Japanese Ministry of Education, Culture, Sports, Science and Technology (MEXT) and Japan Society for the Promotion of Science (JSPS) KAKENHI, Japan; Consejo Nacional de Ciencia (CONACYT) y Tecnología, through Fondo de Cooperación Internacional en Ciencia y Tecnología (FONCICYT) and Dirección General de Asuntos del Personal Academico (DGAPA), Mexico; Nederlandse Organisatie voor Wetenschappelijk Onderzoek (NWO), Netherlands; The Research Council of Norway, Norway; Commission on Science and Technology for Sustainable Development in the South (COMSATS), Pakistan; Pontificia Universidad Católica del Perú, Peru; Ministry of Education and Science, National Science Centre and WUT ID-UB, Poland; Korea Institute of Science and Technology Information and National Research Foundation of Korea (NRF), Republic of Korea; Ministry of Education and Scientific Research, Institute of Atomic Physics and Ministry of Research and Innovation and Institute of Atomic Physics, Romania; Joint Institute for Nuclear Research (JINR), Ministry of Education and Science of the Russian Federation, National Research Centre Kurchatov Institute, Russian Science Foundation and Russian Foundation for Basic Research, Russia; Ministry of Education, Science, Research and Sport of the Slovak Republic, Slovakia; National Research Foundation of South Africa, South Africa; Swedish Research Council (VR) and Knut & Alice Wallenberg Foundation (KAW), Sweden; European Organization for Nuclear Research, Switzerland; Suranaree University of Technology (SUT), National Science and Technology Development Agency (NSDTA) and Office of the Higher Education Commission under NRU project of Thailand, Thailand; Turkish Atomic Energy Agency (TAEK), Turkey; National Academy of Sciences of Ukraine, Ukraine; Science and Technology Facilities Council (STFC), United Kingdom; National Science Foundation of the United States of America (NSF) and United States Department of Energy, Office of Nuclear Physics (DOE NP), United States of America.

References

[1] N. Brambilla *et al.*, "QCD and strongly coupled gauge theories: challenges and perspectives," *Eur. Phys. J. C* **74** no. 10, (2014) 2981, arXiv:1404.3723 [hep-ph].

[2] C. Salgado *et al.*, "Proton–nucleus collisions at the LHC: Scientific opportunities and requirements," *J. Phys. G* **39** (2012) 015010, arXiv:1105.3919 [hep-ph].

[3] **ALICE** Collaboration, B. Abelev *et al.*, "Transverse momentum dependence of inclusive primary charged-particle production in p–Pb collisions at $\sqrt{s_{\mathrm{NN}}} = 5.02$ TeV," *Eur. Phys. J. C* **74** no. 9, (2014) 3054, arXiv:1405.2737 [nucl-ex].

[4] **ATLAS** Collaboration, G. Aad *et al.*, "Transverse momentum, rapidity, and centrality dependence of inclusive charged-particle production in $\sqrt{s_{\mathrm{NN}}} = 5.02$ TeV p–Pb collisions measured by the ATLAS experiment," *Phys. Lett. B* **763** (2016) 313–336, arXiv:1605.06436 [hep-ex].

[5] **CMS** Collaboration, V. Khachatryan *et al.*, "Charged-particle nuclear modification factors in Pb–Pb and p–Pb collisions at $\sqrt{s_{\mathrm{NN}}} = 5.02$ TeV," *JHEP* **04** (2017) 039, arXiv:1611.01664 [nucl-ex].

[6] **ALICE** Collaboration, S. Acharya *et al.*, "Neutral pion and η meson production in p–Pb collisions at $\sqrt{s_{\mathrm{NN}}} = 5.02$ TeV," *Eur. Phys. J. C* **78** no. 8, (2018) 624, arXiv:1801.07051 [nucl-ex].

[7] **PHENIX** Collaboration, S. Adler *et al.*, "Absence of suppression in particle production at large transverse momentum in $\sqrt{s_{\mathrm{NN}}} = 200$ GeV d–Au collisions," *Phys. Rev. Lett.* **91** (2003) 072303, arXiv:nucl-ex/0306021.

[8] **STAR** Collaboration, J. Adams *et al.*, "Evidence from d–Au measurements for final state suppression of high p_{T} hadrons in Au–Au collisions at RHIC," *Phys. Rev. Lett.* **91** (2003) 072304, arXiv:nucl-ex/0306024.

[9] K. Kovarik *et al.*, "nCTEQ15 - Global analysis of nuclear parton distributions with uncertainties in the CTEQ framework," *Phys. Rev. D* **93** no. 8, (2016) 085037, arXiv:1509.00792 [hep-ph].

[10] K. J. Eskola, P. Paakkinen, H. Paukkunen, and C. A. Salgado, "EPPS16: Nuclear parton distributions with LHC data," *Eur. Phys. J. C* **77** no. 3, (2017) 163, arXiv:1612.05741 [hep-ph].

[11] F. Gelis, E. Iancu, J. Jalilian-Marian, and R. Venugopalan, "The Color Glass Condensate," *Ann. Rev. Nucl. Part. Sci.* **60** (2010) 463–489, arXiv:1002.0333 [hep-ph].

[12] T. Lappi and H. Mäntysaari, "Single inclusive particle production at high energy from HERA data to proton–nucleus collisions," *Phys. Rev. D* **88** (2013) 114020, arXiv:1309.6963 [hep-ph].

[13] F. Arleo, F. Cougoulic, and S. Peigné, "Fully coherent energy loss effects on light hadron production in pA collisions," *JHEP* **09** (2020) 190, arXiv:2003.06337 [hep-ph].

[14] I. Vitev, "Non-Abelian energy loss in cold nuclear matter," *Phys. Rev. C* **75** (2007) 064906, arXiv:hep-ph/0703002.

[15] **ALICE** Collaboration, K. Aamodt *et al.*, "The ALICE experiment at the CERN LHC," *JINST* **3** (2008) S08002.

[16] **ALICE** Collaboration, B. Abelev *et al.*, "Performance of the ALICE Experiment at the CERN LHC," *Int. J. Mod. Phys.* **A29** (2014) 1430044, arXiv:1402.4476 [nucl-ex].

[17] **ALICE** Collaboration, K. Aamodt *et al.*, "Alignment of the ALICE Inner Tracking System with cosmic-ray tracks," *JINST* **5** (2010) P03003, arXiv:1001.0502 [physics.ins-det].

[18] **ALICE EMCal** Collaboration, U. Abeysekara *et al.*, "ALICE EMCal Physics Performance Report," arXiv:1008.0413 [physics.ins-det].

[19] J. Allen *et al.*, "ALICE DCal: An Addendum to the EMCal Technical Design Report Di-Jet and Hadron-Jet correlation measurements in ALICE," CERN-LHCC-2010-011. ALICE-TDR-14-add-1. http://cds.cern.ch/record/1272952.

[20] **ALICE** Collaboration, G. Dellacasa *et al.*, "ALICE technical design report of the photon spectrometer (PHOS)," CERN-LHCC-99-04. http://cds.cern.ch/record/381432.

[21] **ALICE** Collaboration, E. Abbas *et al.*, "Performance of the ALICE VZERO system," *JINST* **8** (2013) P10016, arXiv:1306.3130 [nucl-ex].

[22] **ALICE** Collaboration, S. Acharya *et al.*, "π^0 and η meson production in proton–proton collisions at $\sqrt{s} = 8$ TeV," *Eur. Phys. J. C* **78** no. 3, (2018) 263, arXiv:1708.08745 [hep-ex].

[23] *see supplemental material in appendix.*

[24] **ALICE** Collaboration, C. W. Fabjan *et al.*, "ALICE: Physics performance report, volume II," *J. Phys. G* **32** (2006) 1295–2040.

[25] **ALICE** Collaboration, S. Acharya *et al.*, "Measurement of the inclusive isolated photon production cross section in pp collisions at $\sqrt{s}$ = 7 TeV," *Eur. Phys. J. C* **79** no. 11, (2019) 896, arXiv:1906.01371 [nucl-ex].

[26] **ALICE** Collaboration, S. Acharya *et al.*, "Calibration of the photon spectrometer PHOS of the ALICE experiment," *JINST* **14** no. 05, (2019) P05025, arXiv:1902.06145 [physics.ins-det].

[27] **ALICE** Collaboration, S. Acharya *et al.*, "Production of π^0 and η mesons up to high transverse momentum in pp collisions at 2.76 TeV," *Eur. Phys. J. C* **77** no. 5, (2017) 339, arXiv:1702.00917 [hep-ex].

[28] H.-L. Lai, M. Guzzi, J. Huston, Z. Li, P. M. Nadolsky, J. Pumplin, and C.-P. Yuan, "New parton distributions for collider physics," *Phys. Rev. D* **82** (2010) 074024, arXiv:1007.2241 [hep-ph].

[29] D. de Florian, R. Sassot, M. Epele, R. J. Hernández-Pinto, and M. Stratmann, "Parton-to-pion fragmentation reloaded," *Phys. Rev.* **D91** no. 1, (2015) 014035, arXiv:1410.6027 [hep-ph].

[30] C. A. Aidala, F. Ellinghaus, R. Sassot, J. P. Seele, and M. Stratmann, "Global analysis of fragmentation functions for η mesons," *Phys. Rev.* **D83** (2011) 034002, arXiv:1009.6145 [hep-ph].

[31] W. Tung, H. Lai, A. Belyaev, J. Pumplin, D. Stump, and C.-P. Yuan, "Heavy quark mass effects in deep inelastic Ssattering and global QCD analysis," *JHEP* **02** (2007) 053, arXiv:hep-ph/0611254.

[32] T. Sjostrand, S. Mrenna, and P. Z. Skands, "A brief introduction to PYTHIA 8.1," *Comput. Phys. Commun.* **178** (2008) 852–867, arXiv:0710.3820 [hep-ph].

[33] P. Skands, S. Carrazza, and J. Rojo, "Tuning PYTHIA 8.1: the Monash 2013 Tune," *Eur. Phys. J. C* **74** no. 8, (2014) 3024, arXiv:1404.5630 [hep-ph].

[34] S. Alioli, P. Nason, C. Oleari, and E. Re, "A general framework for implementing NLO calculations in shower Monte Carlo programs: the POWHEG BOX," *JHEP* **06** (2010) 043, arXiv:1002.2581 [hep-ph].

[35] S. Alioli, P. Nason, C. Oleari, and E. Re, "NLO vector-boson production matched with shower in POWHEG," *JHEP* **07** (2008) 060, arXiv:0805.4802 [hep-ph].

[36] R. Brun, F. Bruyant, F. Carminati, S. Giani, M. Maire, A. McPherson, G. Patrick, and L. Urban, "GEANT: Detector Description and Simulation Tool," CERN-W5013. https://cds.cern.ch/record/1082634.

[37] S. Roesler, R. Engel, and J. Ranft, "The Monte Carlo event generator DPMJET-III," in *International Conference on Advanced Monte Carlo for Radiation Physics, Particle Transport Simulation and Applications (MC 2000)*, pp. 1033–1038. 12, 2000. arXiv:hep-ph/0012252.

[38] **ALICE** Collaboration, S. Acharya *et al.*, "Direct photon production at low transverse momentum in proton-proton collisions at $\sqrt{s} = 2.76$ and 8 TeV," *Phys. Rev. C* **99** no. 2, (2019) 024912, arXiv:1803.09857 [nucl-ex].

[39] G. Lafferty and T. Wyatt, "Where to stick your data points: The treatment of measurements within wide bins," *Nucl. Instrum. Meth. A* **355** (1995) 541–547.

[40] A. Valassi and R. Chierici, "Information and treatment of unknown correlations in the combination of measurements using the BLUE method," *Eur. Phys. J. C* **74** (2014) 2717, arXiv:1307.4003 [physics.data-an].

[41] L. Lyons, D. Gibaut, and P. Clifford, "How to combine correlated estimates of a single physical quantity," *Nucl. Instrum. Meth. A* **270** (1988) 110.

[42] A. Bylinkin, N. S. Chernyavskaya, and A. A. Rostovtsev, "Predictions on the transverse momentum spectra for charged particle production at LHC-energies from a two component model," *Eur. Phys. J. C* **75** no. 4, (2015) 166, arXiv:1501.05235 [hep-ph].

[43] M. Guzzi, P. Nadolsky, E. Berger, H.-L. Lai, F. Olness, and C. P. Yuan, "CT10 parton distributions and other developments in the global QCD analysis," arXiv:1101.0561 [hep-ph].

[44] J. W. Cronin, H. J. Frisch, M. J. Shochet, J. P. Boymond, R. Mermod, P. A. Piroue, and R. L. Sumner, "Production of hadrons with large transverse momentum at 200, 300, and 400 GeV," *Phys. Rev. D* **11** (1975) 3105–3123.

[45] A. H. Rezaeian and Z. Lu, "Cronin effect for protons and pions in high-energy pA collisions," *Nucl. Phys. A* **826** (2009) 198–210, arXiv:0810.4942 [hep-ph].

[46] **ALICE** Collaboration, S. Acharya *et al.*, "Transverse momentum spectra and nuclear modification factors of charged particles in pp, p–Pb and Pb–Pb collisions at the LHC," *JHEP* **11** (2018) 013, arXiv:1802.09145 [nucl-ex].

[47] A. Huss, A. Kurkela, A. Mazeliauskas, R. Paatelainen, W. van der Schee, and U. A. Wiedemann, "Predicting parton energy loss in small collision systems," arXiv:2007.13758 [hep-ph].

[48] **ALICE** Collaboration, S. Acharya *et al.*, "ALICE luminosity determination for p–Pb collisions at $\sqrt{s_{\mathrm{NN}}} = 8.16$ TeV," ALICE-PUBLIC-2018-002. https://cds.cern.ch/record/2314660.

[49] **Particle Data Group** Collaboration, M. Tanabashi *et al.*, "Review of particle physics," *Phys. Rev. D* **98** (Aug, 2018) 030001. https://link.aps.org/doi/10.1103/PhysRevD.98.030001.

A The ALICE Collaboration

S. Acharya[142], D. Adamová[97], A. Adler[75], J. Adolfsson[82], G. Aglieri Rinella[35], M. Agnello[31], N. Agrawal[55], Z. Ahammed[142], S. Ahmad[16], S.U. Ahn[77], I. Ahuja[39], Z. Akbar[52], A. Akindinov[94], M. Al-Turany[109], S.N. Alam[41], D. Aleksandrov[90], B. Alessandro[60], H.M. Alfanda[7], R. Alfaro Molina[72], B. Ali[16], Y. Ali[14], A. Alici[26], N. Alizadehvandchali[126], A. Alkin[35], J. Alme[21], T. Alt[69], L. Altenkamper[21], I. Altsybeev[114], M.N. Anaam[7], C. Andrei[49], D. Andreou[92], A. Andronic[145], M. Angeletti[35], V. Anguelov[106], F. Antinori[58], P. Antonioli[55], C. Anuj[16], N. Apadula[81], L. Aphecetche[116], H. Appelshäuser[69], S. Arcelli[26], R. Arnaldi[60], I.C. Arsene[20], M. Arslandok[147,106], A. Augustinus[35], R. Averbeck[109], S. Aziz[79], M.D. Azmi[16], A. Badalà[57], Y.W. Baek[42], X. Bai[109], R. Bailhache[69], Y. Bailung[51], R. Bala[103], A. Balbino[31], A. Baldisseri[139], M. Ball[44], D. Banerjee[4], R. Barbera[27], L. Barioglio[107,25], M. Barlou[86], G.G. Barnaföldi[146], L.S. Barnby[96], V. Barret[136], C. Bartels[129], K. Barth[35], E. Bartsch[69], F. Baruffaldi[28], N. Bastid[136], S. Basu[82], G. Batigne[116], B. Batyunya[76], D. Bauri[50], J.L. Bazo Alba[113], I.G. Bearden[91], C. Beattie[147], I. Belikov[138], A.D.C. Bell Hechavarria[145], F. Bellini[26,35], R. Bellwied[126], S. Belokurova[114], V. Belyaev[95], G. Bencedi[70], S. Beole[25], A. Bercuci[49], Y. Berdnikov[100], A. Berdnikova[106], D. Berenyi[146], L. Bergmann[106], M.G. Besoiu[68], L. Betev[35], P.P. Bhaduri[142], A. Bhasin[103], I.R. Bhat[103], M.A. Bhat[4], B. Bhattacharjee[43], P. Bhattacharya[23], L. Bianchi[25], N. Bianchi[53], J. Bielčík[38], J. Bielčíková[97], J. Biernat[119], A. Bilandzic[107], G. Biro[146], S. Biswas[4], J.T. Blair[120], D. Blau[90], M.B. Blidaru[109], C. Blume[69], G. Boca[29], F. Bock[98], A. Bogdanov[95], S. Boi[23], J. Bok[62], L. Boldizsár[146], A. Bolozdynya[95], M. Bombara[39], P.M. Bond[35], G. Bonomi[141], H. Borel[139], A. Borissov[83], H. Bossi[147], E. Botta[25], L. Bratrud[69], P. Braun-Munzinger[109], M. Bregant[122], M. Broz[38], G.E. Bruno[108,34], M.D. Buckland[129], D. Budnikov[110], H. Buesching[69], S. Bufalino[31], O. Bugnon[116], P. Buhler[115], Z. Buthelezi[73,133], J.B. Butt[14], S.A. Bysiak[119], D. Caffarri[92], M. Cai[28,7], H. Caines[147], A. Caliva[109], E. Calvo Villar[113], J.M.M. Camacho[121], R.S. Camacho[46], P. Camerini[24], F.D.M. Canedo[122], A.A. Capon[115], F. Carnesecchi[35,26], R. Caron[139], J. Castillo Castellanos[139], E.A.R. Casula[23], F. Catalano[31], C. Ceballos Sanchez[76], P. Chakraborty[50], S. Chandra[142], S. Chapeland[35], M. Chartier[129], S. Chattopadhyay[142], S. Chattopadhyay[111], A. Chauvin[23], T.G. Chavez[46], C. Cheshkov[137], B. Cheynis[137], V. Chibante Barroso[35], D.D. Chinellato[123], S. Cho[62], P. Chochula[35], P. Christakoglou[92], C.H. Christensen[91], P. Christiansen[82], T. Chujo[135], C. Cicalo[56], L. Cifarelli[26], F. Cindolo[55], M.R. Ciupek[109], G. Clai[II,55], J. Cleymans[I,125], F. Colamaria[54], J.S. Colburn[112], D. Colella[108,54,34,146], A. Collu[81], M. Colocci[35,26], M. Concas[III,60], G. Conesa Balbastre[80], Z. Conesa del Valle[79], G. Contin[24], J.G. Contreras[38], T.M. Cormier[98], P. Cortese[32], M.R. Cosentino[124], F. Costa[35], S. Costanza[29], P. Crochet[136], E. Cuautle[70], P. Cui[7], L. Cunqueiro[98], A. Dainese[58], F.P.A. Damas[116,139], M.C. Danisch[106], A. Danu[68], I. Das[111], P. Das[88], P. Das[4], S. Das[4], S. Dash[50], S. De[88], A. De Caro[30], G. de Cataldo[54], L. De Cilladi[25], J. de Cuveland[40], A. De Falco[23], D. De Gruttola[30], N. De Marco[60], C. De Martin[24], S. De Pasquale[30], S. Deb[51], H.F. Degenhardt[122], K.R. Deja[143], L. Dello Stritto[30], S. Delsanto[25], W. Deng[7], P. Dhankher[19], D. Di Bari[34], A. Di Mauro[35], R.A. Diaz[8], T. Dietel[125], Y. Ding[137,7], R. Divià[35], D.U. Dixit[19], Ø. Djuvsland[21], U. Dmitrieva[64], J. Do[62], A. Dobrin[68], B. Dönigus[69], O. Dordic[20], A.K. Dubey[142], A. Dubla[109,92], S. Dudi[102], M. Dukhishyam[88], P. Dupieux[136], N. Dzalaiova[13], T.M. Eder[145], R.J. Ehlers[98], V.N. Eikeland[21], D. Elia[54], B. Erazmus[116], F. Ercolessi[26], F. Erhardt[101], A. Erokhin[114], M.R. Ersdal[21], B. Espagnon[79], G. Eulisse[35], D. Evans[112], S. Evdokimov[93], L. Fabbietti[107], M. Faggin[28], J. Faivre[80], F. Fan[7], A. Fantoni[53], M. Fasel[98], P. Fecchio[31], A. Feliciello[60], G. Feofilov[114], A. Fernández Téllez[46], A. Ferrero[139], A. Ferretti[25], V.J.G. Feuillard[106], J. Figiel[119], S. Filchagin[110], D. Finogeev[64], F.M. Fionda[56,21], G. Fiorenza[35,108], F. Flor[126], A.N. Flores[120], S. Foertsch[73], P. Foka[109], S. Fokin[90], E. Fragiacomo[61], E. Frajna[146], U. Fuchs[35], N. Funicello[30], C. Furget[80], A. Furs[64], J.J. Gaardhøje[91], M. Gagliardi[25], A.M. Gago[113], A. Gal[138], C.D. Galvan[121], P. Ganoti[86], C. Garabatos[109], J.R.A. Garcia[46], E. Garcia-Solis[10], K. Garg[116], C. Gargiulo[35], A. Garibli[89], K. Garner[145], P. Gasik[109], E.F. Gauger[120], A. Gautam[128], M.B. Gay Ducati[71], M. Germain[116], J. Ghosh[111], P. Ghosh[142], S.K. Ghosh[4], M. Giacalone[26], P. Gianotti[53], P. Giubellino[109,60], P. Giubilato[28], A.M.C. Glaenzer[139],

P. Glässel[106], V. Gonzalez[144], L.H. González-Trueba[72], S. Gorbunov[40], L. Görlich[119], S. Gotovac[36], V. Grabski[72], L.K. Graczykowski[143], L. Greiner[81], A. Grelli[63], C. Grigoras[35], V. Grigoriev[95], A. Grigoryan[I,1], S. Grigoryan[76,1], O.S. Groettvik[21], F. Grosa[35,60], J.F. Grosse-Oetringhaus[35], R. Grosso[109], G.G. Guardiano[123], R. Guernane[80], M. Guilbaud[116], M. Guittiere[116], K. Gulbrandsen[91], T. Gunji[134], A. Gupta[103], R. Gupta[103], I.B. Guzman[46], S.P. Guzman[46], L. Gyulai[146], M.K. Habib[109], C. Hadjidakis[79], H. Hamagaki[84], G. Hamar[146], M. Hamid[7], R. Hannigan[120], M.R. Haque[143,88], A. Harlenderova[109], J.W. Harris[147], A. Harton[10], J.A. Hasenbichler[35], H. Hassan[98], D. Hatzifotiadou[55], P. Hauer[44], L.B. Havener[147], S. Hayashi[134], S.T. Heckel[107], E. Hellbär[69], H. Helstrup[37], T. Herman[38], E.G. Hernandez[46], G. Herrera Corral[9], F. Herrmann[145], K.F. Hetland[37], H. Hillemanns[35], C. Hills[129], B. Hippolyte[138], B. Hofman[63], B. Hohlweger[92,107], J. Honermann[145], G.H. Hong[148], D. Horak[38], S. Hornung[109], R. Hosokawa[15], P. Hristov[35], C. Huang[79], C. Hughes[132], P. Huhn[69], T.J. Humanic[99], H. Hushnud[111], L.A. Husova[145], N. Hussain[43], D. Hutter[40], J.P. Iddon[35,129], R. Ilkaev[110], H. Ilyas[14], M. Inaba[135], G.M. Innocenti[35], M. Ippolitov[90], A. Isakov[38,97], M.S. Islam[111], M. Ivanov[109], V. Ivanov[100], V. Izucheev[93], B. Jacak[81], N. Jacazio[35], P.M. Jacobs[81], S. Jadlovska[118], J. Jadlovsky[118], S. Jaelani[63], C. Jahnke[123,122], M.J. Jakubowska[143], M.A. Janik[143], T. Janson[75], M. Jercic[101], O. Jevons[112], F. Jonas[98,145], P.G. Jones[112], J.M. Jowett [35,109], J. Jung[69], M. Jung[69], A. Junique[35], A. Jusko[112], J. Kaewjai[117], P. Kalinak[65], A. Kalweit[35], V. Kaplin[95], S. Kar[7], A. Karasu Uysal[78], D. Karatovic[101], O. Karavichev[64], T. Karavicheva[64], P. Karczmarczyk[143], E. Karpechev[64], A. Kazantsev[90], U. Kebschull[75], R. Keidel[48], D.L.D. Keijdener[63], M. Keil[35], B. Ketzer[44], Z. Khabanova[92], A.M. Khan[7], S. Khan[16], A. Khanzadeev[100], Y. Kharlov[93], A. Khatun[16], A. Khuntia[119], B. Kileng[37], B. Kim[17,62], D. Kim[148], D.J. Kim[127], E.J. Kim[74], J. Kim[148], J.S. Kim[42], J. Kim[106], J. Kim[148], J. Kim[74], M. Kim[106], S. Kim[18], T. Kim[148], S. Kirsch[69], I. Kisel[40], S. Kiselev[94], A. Kisiel[143], J.L. Klay[6], J. Klein[35], S. Klein[81], C. Klein-Bösing[145], M. Kleiner[69], T. Klemenz[107], A. Kluge[35], A.G. Knospe[126], C. Kobdaj[117], M.K. Köhler[106], T. Kollegger[109], A. Kondratyev[76], N. Kondratyeva[95], E. Kondratyuk[93], J. Konig[69], S.A. Konigstorfer[107], P.J. Konopka[35,2], G. Kornakov[143], S.D. Koryciak[2], L. Koska[118], A. Kotliarov[97], O. Kovalenko[87], V. Kovalenko[114], M. Kowalski[119], I. Králik[65], A. Kravčáková[39], L. Kreis[109], M. Krivda[112,65], F. Krizek[97], K. Krizkova Gajdosova[38], M. Kroesen[106], M. Krüger[69], E. Kryshen[100], M. Krzewicki[40], V. Kučera[35], C. Kuhn[138], P.G. Kuijer[92], T. Kumaoka[135], D. Kumar[142], L. Kumar[102], N. Kumar[102], S. Kundu[35,88], P. Kurashvili[87], A. Kurepin[64], A.B. Kurepin[64], A. Kuryakin[110], S. Kushpil[97], J. Kvapil[112], M.J. Kweon[62], J.Y. Kwon[62], Y. Kwon[148], S.L. La Pointe[40], P. La Rocca[27], Y.S. Lai[81], A. Lakrathok[117], M. Lamanna[35], R. Langoy[131], K. Lapidus[35], P. Larionov[53], E. Laudi[35], L. Lautner[35,107], R. Lavicka[38], T. Lazareva[114], R. Lea[141,24], J. Lee[135], J. Lehrbach[40], R.C. Lemmon[96], I. León Monzón[121], E.D. Lesser[19], M. Lettrich[35,107], P. Lévai[146], X. Li[11], X.L. Li[7], J. Lien[131], R. Lietava[112], B. Lim[17], S.H. Lim[17], V. Lindenstruth[40], A. Lindner[49], C. Lippmann[109], A. Liu[19], J. Liu[129], I.M. Lofnes[21], V. Loginov[95], C. Loizides[98], P. Loncar[36], J.A. Lopez[106], X. Lopez[136], E. López Torres[8], J.R. Luhder[145], M. Lunardon[28], G. Luparello[61], Y.G. Ma[41], A. Maevskaya[64], M. Mager[35], T. Mahmoud[44], A. Maire[138], M. Malaev[100], Q.W. Malik[20], L. Malinina[IV,76], D. Mal'Kevich[94], N. Mallick[51], P. Malzacher[109], G. Mandaglio[33,57], V. Manko[90], F. Manso[136], V. Manzari[54], Y. Mao[7], J. Mareš[67], G.V. Margagliotti[24], A. Margotti[55], A. Marín[109], C. Markert[120], M. Marquard[69], N.A. Martin[106], P. Martinengo[35], J.L. Martinez[126], M.I. Martínez[46], G. Martínez García[116], S. Masciocchi[109], M. Masera[25], A. Masoni[56], L. Massacrier[79], A. Mastroserio[140,54], A.M. Mathis[107], O. Matonoha[82], P.F.T. Matuoka[122], A. Matyja[119], C. Mayer[119], A.L. Mazuecos[35], F. Mazzaschi[25], M. Mazzilli[35,54], M.A. Mazzoni[59], J.E. Mdhluli[133], A.F. Mechler[69], F. Meddi[22], Y. Melikyan[64], A. Menchaca-Rocha[72], E. Meninno[115,30], A.S. Menon[126], M. Meres[13], S. Mhlanga[125,73], Y. Miake[135], L. Micheletti[25], L.C. Migliorin[137], D.L. Mihaylov[107], K. Mikhaylov[76,94], A.N. Mishra[146], D. Miśkowiec[109], A. Modak[4], A.P. Mohanty[63], B. Mohanty[88], M. Mohisin Khan[16], Z. Moravcova[91], C. Mordasini[107], D.A. Moreira De Godoy[145], L.A.P. Moreno[46], I. Morozov[64], A. Morsch[35], T. Mrnjavac[35], V. Muccifora[53], E. Mudnic[36], D. Mühlheim[145], S. Muhuri[142], J.D. Mulligan[81], A. Mulliri[23], M.G. Munhoz[122], R.H. Munzer[69], H. Murakami[134], S. Murray[125], L. Musa[35], J. Musinsky[65], C.J. Myers[126], J.W. Myrcha[143], B. Naik[50], R. Nair[87], B.K. Nandi[50], R. Nania[55],

E. Nappi[54], M.U. Naru[14], A.F. Nassirpour[82], A. Nath[106], C. Nattrass[132], A. Neagu[20], L. Nellen[70], S.V. Nesbo[37], G. Neskovic[40], D. Nesterov[114], B.S. Nielsen[91], S. Nikolaev[90], S. Nikulin[90], V. Nikulin[100], F. Noferini[55], S. Noh[12], P. Nomokonov[76], J. Norman[129], N. Novitzky[135], P. Nowakowski[143], A. Nyanin[90], J. Nystrand[21], M. Ogino[84], A. Ohlson[82], V.A. Okorokov[95], J. Oleniacz[143], A.C. Oliveira Da Silva[132], M.H. Oliver[147], A. Onnerstad[127], C. Oppedisano[60], A. Ortiz Velasquez[70], T. Osako[47], A. Oskarsson[82], J. Otwinowski[119], K. Oyama[84], Y. Pachmayer[106], S. Padhan[50], D. Pagano[141], G. Paić[70], A. Palasciano[54], J. Pan[144], S. Panebianco[139], P. Pareek[142], J. Park[62], J.E. Parkkila[127], S.P. Pathak[126], R.N. Patra[103,35], B. Paul[23], J. Pazzini[141], H. Pei[7], T. Peitzmann[63], X. Peng[7], L.G. Pereira[71], H. Pereira Da Costa[139], D. Peresunko[90], G.M. Perez[8], S. Perrin[139], Y. Pestov[5], V. Petráček[38], M. Petrovici[49], R.P. Pezzi[71], S. Piano[61], M. Pikna[13], P. Pillot[116], O. Pinazza[55,35], L. Pinsky[126], C. Pinto[27], S. Pisano[53], M. Płoskoń[81], M. Planinic[101], F. Pliquett[69], M.G. Poghosyan[98], B. Polichtchouk[93], S. Politano[31], N. Poljak[101], A. Pop[49], S. Porteboeuf-Houssais[136], J. Porter[81], V. Pozdniakov[76], S.K. Prasad[4], R. Preghenella[55], F. Prino[60], C.A. Pruneau[144], I. Pshenichnov[64], M. Puccio[35], S. Qiu[92], L. Quaglia[25], R.E. Quishpe[126], S. Ragoni[112], A. Rakotozafindrabe[139], L. Ramello[32], F. Rami[138], S.A.R. Ramirez[46], A.G.T. Ramos[34], R. Raniwala[104], S. Raniwala[104], S.S. Räsänen[45], R. Rath[51], I. Ravasenga[92], K.F. Read[98,132], A.R. Redelbach[40], K. Redlich[V,87], A. Rehman[21], P. Reichelt[69], F. Reidt[35], H.A. Reme-ness[37], R. Renfordt[69], Z. Rescakova[39], K. Reygers[106], A. Riabov[100], V. Riabov[100], T. Richert[82,91], M. Richter[20], W. Riegler[35], F. Riggi[27], C. Ristea[68], S.P. Rode[51], M. Rodríguez Cahuantzi[46], K. Røed[20], R. Rogalev[93], E. Rogochaya[76], T.S. Rogoschinski[69], D. Rohr[35], D. Röhrich[21], P.F. Rojas[46], P.S. Rokita[143], F. Ronchetti[53], A. Rosano[33,57], E.D. Rosas[70], A. Rossi[58], A. Rotondi[29], A. Roy[51], P. Roy[111], S. Roy[50], N. Rubini[26], O.V. Rueda[82], R. Rui[24], B. Rumyantsev[76], A. Rustamov[89], E. Ryabinkin[90], Y. Ryabov[100], A. Rybicki[119], H. Rytkonen[127], W. Rzesa[143], O.A.M. Saarimaki[45], R. Sadek[116], S. Sadovsky[93], J. Saetre[21], K. Šafařík[38], S.K. Saha[142], S. Saha[88], B. Sahoo[50], P. Sahoo[50], R. Sahoo[51], S. Sahoo[66], D. Sahu[51], P.K. Sahu[66], J. Saini[142], S. Sakai[135], S. Sambyal[103], V. Samsonov[I,100,95], D. Sarkar[144], N. Sarkar[142], P. Sarma[43], V.M. Sarti[107], M.H.P. Sas[147], J. Schambach[98,120], H.S. Scheid[69], C. Schiaua[49], R. Schicker[106], A. Schmah[106], C. Schmidt[109], H.R. Schmidt[105], M.O. Schmidt[106], M. Schmidt[105], N.V. Schmidt[98,69], A.R. Schmier[132], R. Schotter[138], J. Schukraft[35], Y. Schutz[138], K. Schwarz[109], K. Schweda[109], G. Scioli[26], E. Scomparin[60], J.E. Seger[15], Y. Sekiguchi[134], D. Sekihata[134], I. Selyuzhenkov[109,95], S. Senyukov[138], J.J. Seo[62], D. Serebryakov[64], L. Šerkšnytė[107], A. Sevcenco[68], T.J. Shaba[73], A. Shabanov[64], A. Shabetai[116], R. Shahoyan[35], W. Shaikh[111], A. Shangaraev[93], A. Sharma[102], H. Sharma[119], M. Sharma[103], N. Sharma[102], S. Sharma[103], O. Sheibani[126], K. Shigaki[47], M. Shimomura[85], S. Shirinkin[94], Q. Shou[41], Y. Sibiriak[90], S. Siddhanta[56], T. Siemiarczuk[87], T.F. Silva[122], D. Silvermyr[82], G. Simonetti[35], B. Singh[107], R. Singh[88], R. Singh[103], R. Singh[51], V.K. Singh[142], V. Singhal[142], T. Sinha[111], B. Sitar[13], M. Sitta[32], T.B. Skaali[20], G. Skorodumovs[106], M. Slupecki[45], N. Smirnov[147], R.J.M. Snellings[63], C. Soncco[113], J. Song[126], A. Songmoolnak[117], F. Soramel[28], S. Sorensen[132], I. Sputowska[119], J. Stachel[106], I. Stan[68], P.J. Steffanic[132], S.F. Stiefelmaier[106], D. Stocco[116], I. Storehaug[20], M.M. Storetvedt[37], C.P. Stylianidis[92], A.A.P. Suaide[122], T. Sugitate[47], C. Suire[79], M. Suljic[35], R. Sultanov[94], M. Šumbera[97], V. Sumberia[103], S. Sumowidagdo[52], S. Swain[66], A. Szabo[13], I. Szarka[13], U. Tabassam[14], S.F. Taghavi[107], G. Taillepied[136], J. Takahashi[123], G.J. Tambave[21], S. Tang[136,7], Z. Tang[130], M. Tarhini[116], M.G. Tarzila[49], A. Tauro[35], G. Tejeda Muñoz[46], A. Telesca[35], L. Terlizzi[25], C. Terrevoli[126], G. Tersimonov[3], S. Thakur[142], D. Thomas[120], R. Tieulent[137], A. Tikhonov[64], A.R. Timmins[126], M. Tkacik[118], A. Toia[69], N. Topilskaya[64], M. Toppi[53], F. Torales-Acosta[19], S.R. Torres[38], A. Trifiró[33,57], S. Tripathy[55,70], T. Tripathy[50], S. Trogolo[35,28], G. Trombetta[34], V. Trubnikov[3], W.H. Trzaska[127], T.P. Trzcinski[143], B.A. Trzeciak[38], A. Tumkin[110], R. Turrisi[58], T.S. Tveter[20], K. Ullaland[21], A. Uras[137], M. Urioni[141], G.L. Usai[23], M. Vala[39], N. Valle[29], S. Vallero[60], N. van der Kolk[63], L.V.R. van Doremalen[63], M. van Leeuwen[92], P. Vande Vyvre[35], D. Varga[146], Z. Varga[146], M. Varga-Kofarago[146], A. Vargas[46], M. Vasileiou[86], A. Vasiliev[90], O. Vázquez Doce[107], V. Vechernin[114], E. Vercellin[25], S. Vergara Limón[46], L. Vermunt[63], R. Vértesi[146], M. Verweij[63], L. Vickovic[36], Z. Vilakazi[133], O. Villalobos Baillie[112], G. Vino[54], A. Vinogradov[90], T. Virgili[30],

V. Vislavicius[91], A. Vodopyanov[76], B. Volkel[35], M.A. Völkl[106], K. Voloshin[94], S.A. Voloshin[144], G. Volpe[34], B. von Haller[35], I. Vorobyev[107], D. Voscek[118], J. Vrláková[39], B. Wagner[21], C. Wang[41], D. Wang[41], M. Weber[115], A. Wegrzynek[35], S.C. Wenzel[35], J.P. Wessels[145], J. Wiechula[69], J. Wikne[20], G. Wilk[87], J. Wilkinson[109], G.A. Willems[145], E. Willsher[112], B. Windelband[106], M. Winn[139], W.E. Witt[132], J.R. Wright[120], W. Wu[41], Y. Wu[130], R. Xu[7], S. Yalcin[78], Y. Yamaguchi[47], K. Yamakawa[47], S. Yang[21], S. Yano[47,139], Z. Yin[7], H. Yokoyama[63], I.-K. Yoo[17], J.H. Yoon[62], S. Yuan[21], A. Yuncu[106], V. Zaccolo[24], A. Zaman[14], C. Zampolli[35], H.J.C. Zanoli[63], N. Zardoshti[35], A. Zarochentsev[114], P. Závada[67], N. Zaviyalov[110], H. Zbroszczyk[143], M. Zhalov[100], S. Zhang[41], X. Zhang[7], Y. Zhang[130], V. Zherebchevskii[114], Y. Zhi[11], D. Zhou[7], Y. Zhou[91], J. Zhu[7,109], A. Zichichi[26], G. Zinovjev[3], N. Zurlo[141]

Affiliation Notes

[I] Deceased
[II] Also at: Italian National Agency for New Technologies, Energy and Sustainable Economic Development (ENEA), Bologna, Italy
[III] Also at: Dipartimento DET del Politecnico di Torino, Turin, Italy
[IV] Also at: M.V. Lomonosov Moscow State University, D.V. Skobeltsyn Institute of Nuclear, Physics, Moscow, Russia
[V] Also at: Institute of Theoretical Physics, University of Wroclaw, Poland

Collaboration Institutes

[1] A.I. Alikhanyan National Science Laboratory (Yerevan Physics Institute) Foundation, Yerevan, Armenia
[2] AGH University of Science and Technology, Cracow, Poland
[3] Bogolyubov Institute for Theoretical Physics, National Academy of Sciences of Ukraine, Kiev, Ukraine
[4] Bose Institute, Department of Physics and Centre for Astroparticle Physics and Space Science (CAPSS), Kolkata, India
[5] Budker Institute for Nuclear Physics, Novosibirsk, Russia
[6] California Polytechnic State University, San Luis Obispo, California, United States
[7] Central China Normal University, Wuhan, China
[8] Centro de Aplicaciones Tecnológicas y Desarrollo Nuclear (CEADEN), Havana, Cuba
[9] Centro de Investigación y de Estudios Avanzados (CINVESTAV), Mexico City and Mérida, Mexico
[10] Chicago State University, Chicago, Illinois, United States
[11] China Institute of Atomic Energy, Beijing, China
[12] Chungbuk National University, Cheongju, Republic of Korea
[13] Comenius University Bratislava, Faculty of Mathematics, Physics and Informatics, Bratislava, Slovakia
[14] COMSATS University Islamabad, Islamabad, Pakistan
[15] Creighton University, Omaha, Nebraska, United States
[16] Department of Physics, Aligarh Muslim University, Aligarh, India
[17] Department of Physics, Pusan National University, Pusan, Republic of Korea
[18] Department of Physics, Sejong University, Seoul, Republic of Korea
[19] Department of Physics, University of California, Berkeley, California, United States
[20] Department of Physics, University of Oslo, Oslo, Norway
[21] Department of Physics and Technology, University of Bergen, Bergen, Norway

[22] Dipartimento di Fisica dell'Università 'La Sapienza' and Sezione INFN, Rome, Italy
[23] Dipartimento di Fisica dell'Università and Sezione INFN, Cagliari, Italy
[24] Dipartimento di Fisica dell'Università and Sezione INFN, Trieste, Italy
[25] Dipartimento di Fisica dell'Università and Sezione INFN, Turin, Italy
[26] Dipartimento di Fisica e Astronomia dell'Università and Sezione INFN, Bologna, Italy
[27] Dipartimento di Fisica e Astronomia dell'Università and Sezione INFN, Catania, Italy
[28] Dipartimento di Fisica e Astronomia dell'Università and Sezione INFN, Padova, Italy
[29] Dipartimento di Fisica e Nucleare e Teorica, Università di Pavia, Pavia, Italy
[30] Dipartimento di Fisica 'E.R. Caianiello' dell'Università and Gruppo Collegato INFN, Salerno, Italy
[31] Dipartimento DISAT del Politecnico and Sezione INFN, Turin, Italy
[32] Dipartimento di Scienze e Innovazione Tecnologica dell'Università del Piemonte Orientale and INFN Sezione di Torino, Alessandria, Italy
[33] Dipartimento di Scienze MIFT, Università di Messina, Messina, Italy
[34] Dipartimento Interateneo di Fisica 'M. Merlin' and Sezione INFN, Bari, Italy
[35] European Organization for Nuclear Research (CERN), Geneva, Switzerland
[36] Faculty of Electrical Engineering, Mechanical Engineering and Naval Architecture, University of Split, Split, Croatia
[37] Faculty of Engineering and Science, Western Norway University of Applied Sciences, Bergen, Norway
[38] Faculty of Nuclear Sciences and Physical Engineering, Czech Technical University in Prague, Prague, Czech Republic
[39] Faculty of Science, P.J. Šafárik University, Košice, Slovakia
[40] Frankfurt Institute for Advanced Studies, Johann Wolfgang Goethe-Universität Frankfurt, Frankfurt, Germany
[41] Fudan University, Shanghai, China
[42] Gangneung-Wonju National University, Gangneung, Republic of Korea
[43] Gauhati University, Department of Physics, Guwahati, India
[44] Helmholtz-Institut für Strahlen- und Kernphysik, Rheinische Friedrich-Wilhelms-Universität Bonn, Bonn, Germany
[45] Helsinki Institute of Physics (HIP), Helsinki, Finland
[46] High Energy Physics Group, Universidad Autónoma de Puebla, Puebla, Mexico
[47] Hiroshima University, Hiroshima, Japan
[48] Hochschule Worms, Zentrum für Technologietransfer und Telekommunikation (ZTT), Worms, Germany
[49] Horia Hulubei National Institute of Physics and Nuclear Engineering, Bucharest, Romania
[50] Indian Institute of Technology Bombay (IIT), Mumbai, India
[51] Indian Institute of Technology Indore, Indore, India
[52] Indonesian Institute of Sciences, Jakarta, Indonesia
[53] INFN, Laboratori Nazionali di Frascati, Frascati, Italy
[54] INFN, Sezione di Bari, Bari, Italy
[55] INFN, Sezione di Bologna, Bologna, Italy
[56] INFN, Sezione di Cagliari, Cagliari, Italy
[57] INFN, Sezione di Catania, Catania, Italy
[58] INFN, Sezione di Padova, Padova, Italy
[59] INFN, Sezione di Roma, Rome, Italy
[60] INFN, Sezione di Torino, Turin, Italy
[61] INFN, Sezione di Trieste, Trieste, Italy
[62] Inha University, Incheon, Republic of Korea
[63] Institute for Gravitational and Subatomic Physics (GRASP), Utrecht University/Nikhef, Utrecht, Netherlands

[64] Institute for Nuclear Research, Academy of Sciences, Moscow, Russia
[65] Institute of Experimental Physics, Slovak Academy of Sciences, Košice, Slovakia
[66] Institute of Physics, Homi Bhabha National Institute, Bhubaneswar, India
[67] Institute of Physics of the Czech Academy of Sciences, Prague, Czech Republic
[68] Institute of Space Science (ISS), Bucharest, Romania
[69] Institut für Kernphysik, Johann Wolfgang Goethe-Universität Frankfurt, Frankfurt, Germany
[70] Instituto de Ciencias Nucleares, Universidad Nacional Autónoma de México, Mexico City, Mexico
[71] Instituto de Física, Universidade Federal do Rio Grande do Sul (UFRGS), Porto Alegre, Brazil
[72] Instituto de Física, Universidad Nacional Autónoma de México, Mexico City, Mexico
[73] iThemba LABS, National Research Foundation, Somerset West, South Africa
[74] Jeonbuk National University, Jeonju, Republic of Korea
[75] Johann-Wolfgang-Goethe Universität Frankfurt Institut für Informatik, Fachbereich Informatik und Mathematik, Frankfurt, Germany
[76] Joint Institute for Nuclear Research (JINR), Dubna, Russia
[77] Korea Institute of Science and Technology Information, Daejeon, Republic of Korea
[78] KTO Karatay University, Konya, Turkey
[79] Laboratoire de Physique des 2 Infinis, Irène Joliot-Curie, Orsay, France
[80] Laboratoire de Physique Subatomique et de Cosmologie, Université Grenoble-Alpes, CNRS-IN2P3, Grenoble, France
[81] Lawrence Berkeley National Laboratory, Berkeley, California, United States
[82] Lund University Department of Physics, Division of Particle Physics, Lund, Sweden
[83] Moscow Institute for Physics and Technology, Moscow, Russia
[84] Nagasaki Institute of Applied Science, Nagasaki, Japan
[85] Nara Women's University (NWU), Nara, Japan
[86] National and Kapodistrian University of Athens, School of Science, Department of Physics , Athens, Greece
[87] National Centre for Nuclear Research, Warsaw, Poland
[88] National Institute of Science Education and Research, Homi Bhabha National Institute, Jatni, India
[89] National Nuclear Research Center, Baku, Azerbaijan
[90] National Research Centre Kurchatov Institute, Moscow, Russia
[91] Niels Bohr Institute, University of Copenhagen, Copenhagen, Denmark
[92] Nikhef, National institute for subatomic physics, Amsterdam, Netherlands
[93] NRC Kurchatov Institute IHEP, Protvino, Russia
[94] NRC «Kurchatov»Institute - ITEP, Moscow, Russia
[95] NRNU Moscow Engineering Physics Institute, Moscow, Russia
[96] Nuclear Physics Group, STFC Daresbury Laboratory, Daresbury, United Kingdom
[97] Nuclear Physics Institute of the Czech Academy of Sciences, Řež u Prahy, Czech Republic
[98] Oak Ridge National Laboratory, Oak Ridge, Tennessee, United States
[99] Ohio State University, Columbus, Ohio, United States
[100] Petersburg Nuclear Physics Institute, Gatchina, Russia
[101] Physics department, Faculty of science, University of Zagreb, Zagreb, Croatia
[102] Physics Department, Panjab University, Chandigarh, India
[103] Physics Department, University of Jammu, Jammu, India
[104] Physics Department, University of Rajasthan, Jaipur, India
[105] Physikalisches Institut, Eberhard-Karls-Universität Tübingen, Tübingen, Germany
[106] Physikalisches Institut, Ruprecht-Karls-Universität Heidelberg, Heidelberg, Germany
[107] Physik Department, Technische Universität München, Munich, Germany
[108] Politecnico di Bari and Sezione INFN, Bari, Italy
[109] Research Division and ExtreMe Matter Institute EMMI, GSI Helmholtzzentrum für Schwerionenforschung GmbH, Darmstadt, Germany

[110] Russian Federal Nuclear Center (VNIIEF), Sarov, Russia
[111] Saha Institute of Nuclear Physics, Homi Bhabha National Institute, Kolkata, India
[112] School of Physics and Astronomy, University of Birmingham, Birmingham, United Kingdom
[113] Sección Física, Departamento de Ciencias, Pontificia Universidad Católica del Perú, Lima, Peru
[114] St. Petersburg State University, St. Petersburg, Russia
[115] Stefan Meyer Institut für Subatomare Physik (SMI), Vienna, Austria
[116] SUBATECH, IMT Atlantique, Université de Nantes, CNRS-IN2P3, Nantes, France
[117] Suranaree University of Technology, Nakhon Ratchasima, Thailand
[118] Technical University of Košice, Košice, Slovakia
[119] The Henryk Niewodniczanski Institute of Nuclear Physics, Polish Academy of Sciences, Cracow, Poland
[120] The University of Texas at Austin, Austin, Texas, United States
[121] Universidad Autónoma de Sinaloa, Culiacán, Mexico
[122] Universidade de São Paulo (USP), São Paulo, Brazil
[123] Universidade Estadual de Campinas (UNICAMP), Campinas, Brazil
[124] Universidade Federal do ABC, Santo Andre, Brazil
[125] University of Cape Town, Cape Town, South Africa
[126] University of Houston, Houston, Texas, United States
[127] University of Jyväskylä, Jyväskylä, Finland
[128] University of Kansas, Lawrence, Kansas, United States
[129] University of Liverpool, Liverpool, United Kingdom
[130] University of Science and Technology of China, Hefei, China
[131] University of South-Eastern Norway, Tonsberg, Norway
[132] University of Tennessee, Knoxville, Tennessee, United States
[133] University of the Witwatersrand, Johannesburg, South Africa
[134] University of Tokyo, Tokyo, Japan
[135] University of Tsukuba, Tsukuba, Japan
[136] Université Clermont Auvergne, CNRS/IN2P3, LPC, Clermont-Ferrand, France
[137] Université de Lyon, CNRS/IN2P3, Institut de Physique des 2 Infinis de Lyon , Lyon, France
[138] Université de Strasbourg, CNRS, IPHC UMR 7178, F-67000 Strasbourg, France, Strasbourg, France
[139] Université Paris-Saclay Centre d'Etudes de Saclay (CEA), IRFU, Départment de Physique Nucléaire (DPhN), Saclay, France
[140] Università degli Studi di Foggia, Foggia, Italy
[141] Università di Brescia, Brescia, Italy
[142] Variable Energy Cyclotron Centre, Homi Bhabha National Institute, Kolkata, India
[143] Warsaw University of Technology, Warsaw, Poland
[144] Wayne State University, Detroit, Michigan, United States
[145] Westfälische Wilhelms-Universität Münster, Institut für Kernphysik, Münster, Germany
[146] Wigner Research Centre for Physics, Budapest, Hungary
[147] Yale University, New Haven, Connecticut, United States
[148] Yonsei University, Seoul, Republic of Korea

B Appendix

B.1 Trigger rejection factors and data samples

The trigger rejection factors (RF) for the EMCal triggers are estimated through a fit to the ratio of the cluster energy spectra in their plateau regions above the respective trigger thresholds. Figure B.1 shows these ratios for the low and high threshold EMCal Level-1 triggers EG2 and EG1 with error function fits at high energy (E) according to $RF(p_{\mathrm{T}}) = R_0 + \tau \times \mathrm{erf}\left(\frac{p_{\mathrm{T}}-p_{\mathrm{T},0}}{\sqrt{2}\times a}\right)$, with the global offset R_0, free parameters (τ, $p_{\mathrm{T},0}$, a) and the error function term $\mathrm{erf}(x) = \frac{2}{\sqrt{\pi}}\int_x^\infty e^{-t^2}\mathrm{d}t$.

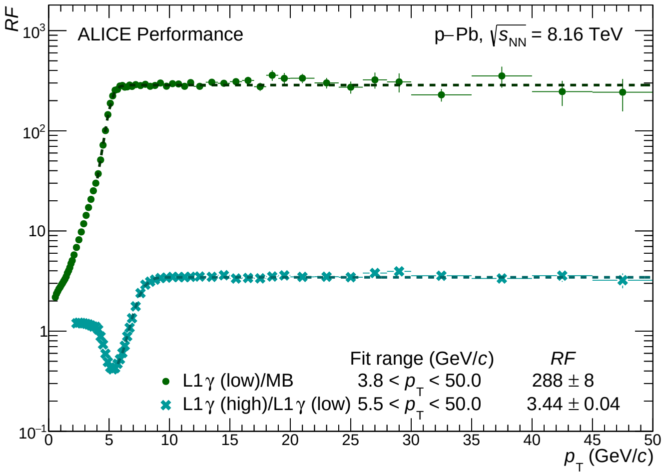

Fig. B.1: Ratio of cluster spectra in EMCal Level-1 triggered data and minimum bias data in p–Pb collisions at $\sqrt{s_{\mathrm{NN}}} = 8.16$ TeV. The dashed lines show the error function fits to the ratios, which are used to obtain the trigger rejection factors RF.

A similar procedure is performed for the PHOS triggers, where RF is determined on the ratio of the corrected π^0 meson spectra instead. The trigger rejection factors from these fits are given in Table B.1 for all event triggers. For the high threshold triggers, RF is obtained from the product $RF_{\mathrm{EG2/MB}} \times RF_{\mathrm{EG1/EG2}}$ or $RF_{\mathrm{PHOS-L0/MB}} \times RF_{\mathrm{PHOS-L1/L0}}$. Uncertainties on RF are given as combined statistical and systematic uncertainties where the latter part was determined via variations of the low E fit range.

			$\mathscr{L}_{\mathrm{int}}$ (nb^{-1})			
System	Trigger	RF	EMC & mEMC	PCM-EMC	PCM	PHOS
p–Pb	MB	-	0.018(0.041)	0.018	0.022	0.036
	EMCal L1 (low)	288 ± 8	0.206 ± 0.005	0.081 ± 0.002	-	-
	EMCal L1 (high)	852 ± 38	5.67 ± 0.16	1.42 ± 0.04	-	-
	PHOS L0	$(1.66 \pm 0.01) \times 10^3$	-	-	-	1.686 ± 0.014
	PHOS L1	$(1.58 \pm 0.03) \times 10^4$	-	-	-	6.42 ± 0.12
pp	MB	-	1.94	1.94	2.17	1.25
	EMCal/PHOS L0	64.6 ± 1.0	39.4 ± 1.0	39.4 ± 1.0	-	136 ± 17
	EMCal L1	$(14.7 \pm 0.6) \times 10^3$	606 ± 16	606 ± 16	-	-

Table B.1: Trigger rejection factor RF and total integrated luminosities based on the individual samples for the different reconstruction methods and triggers in pp collisions at $\sqrt{s} = 8$ TeV and p–Pb collisions at $\sqrt{s_{\mathrm{NN}}} = 8.16$ TeV. The uncertainties reflect the systematic uncertainty of the RF determination. The uncertainty associated with the determination of the MB cross section of 1.9% for p–Pb and 2.6% for pp is not included. The value in brackets corresponds to the high luminosity minimum bias data sample where TPC tracking is not available.

The integrated luminosities of each trigger sample and for each reconstruction method are calculated based on the MB cross section of $\sigma_{\mathrm{MB}} = (2.09(2.10) \pm 0.04)$ b for the p–Pb (Pb–p) collisions [48] as $\mathscr{L}_{\mathrm{int}} = RF \times N_{\mathrm{events}}/\sigma_{\mathrm{MB}}$ and are listed in Table B.1. For PCM-EMC lower integrated lumiosities are reported due to the lack of TPC readout in two thirds of the triggered data. The pp collision data set at a centre-of-mass energy of $\sqrt{s} = 8$ TeV used in this analysis was recorded in 2012 and the respective integrated luminosities are listed in Table B.1.

B.2 Invariant mass and shower shape distributions

The two-photon invariant mass distribution, $M_{\gamma\gamma}$, around the neutral pion and η meson rest mass [49] reconstructed with the PCM, EMC, PCM-EMC and PHOS methods are shown in Figure B.2. For the PHOS technique, the combinatorial background, obtained from event mixing, is subtracted after scaling with a second order polynomial determined on the ratio of signal and background in order to remove its dependence on the detector acceptance. For the remaining techniques, the combinatorial background is subtracted after scaling to the right-hand side of the signal peak. A residual correlated background arising from residual jet-like correlations is contained in the mixed-event subtracted distributions, which can be described by a linear function and subtracted. This linear function is included in the signal fit function, which is defined as

$$y = A \times \left\{ G(M_{\gamma\gamma}) + \exp\left(\frac{M_{\gamma\gamma} - M_{\pi^0,\eta}}{\lambda}\right) \left[1 - G(M_{\gamma\gamma})\right] \theta(M_{\pi^0,\eta} - M_{\gamma\gamma}) \right\} + B + C \times M_{\gamma\gamma} \quad \text{(B.1)}$$

$$\text{with } G(M_{\gamma\gamma}) = \exp\left[-0.5\left(\frac{M_{\gamma\gamma} - M_{\pi^0,\eta}}{\sigma_{M_{\gamma\gamma}}}\right)^2\right], \quad \text{(B.2)}$$

where the signal is described by a Gaussian distribution $G(M_{\gamma\gamma})$ around the mean value $M_{\pi^0,\eta}$ with a width of $\sigma_{M_{\gamma\gamma}}$. A one-sided exponential tail for $M_{\gamma\gamma} < M_{\pi^0,\eta}$ is enabled with a Heaviside function (θ) and describes the smearing of the distribution due to electron bremsstrahlung for PCM or late photon conversions for EMC and PCM-EMC. An additional exponential tail term for $M_{\gamma\gamma} > M_{\pi^0,\eta}$ is introduced for the analysis of the EMCal-triggered data to account for cluster overlap and resolution effects smearing the reconstructed invariant mass to larger values. The residual correlated background is described with the linear function given by $B + C \times M_{\gamma\gamma}$. The combined combinatorial and residual background is indicated in Figure B.2 by open gray circles, while the signal is shown with solid red markers and the signal fit is given by the blue line. The integration ranges for the raw yield extraction are indicated by vertical dashed lines. Figure B.3 shows the invariant mass peak positions and peak widths (FWHM), obtained from the fits according to Equation B.2, for the different reconstruction methods PCM, PHOS, EMC, and PCM-EMC and for both neutral mesons. Example shower shape distributions (σ^2_{long}) used for the mEMC analysis are shown in Figure B.4 for two p_{T} intervals. The top panels visualize the composition of the overall distribution based on PYTHIA 8 Monte Carlo simulations with contributions from the signal (π^0) and from background sources (η, γ, $\mathrm{e}^{\pm}$, and hadrons). The bottom panels shows the performance of the simulation to describe the distribution in data.

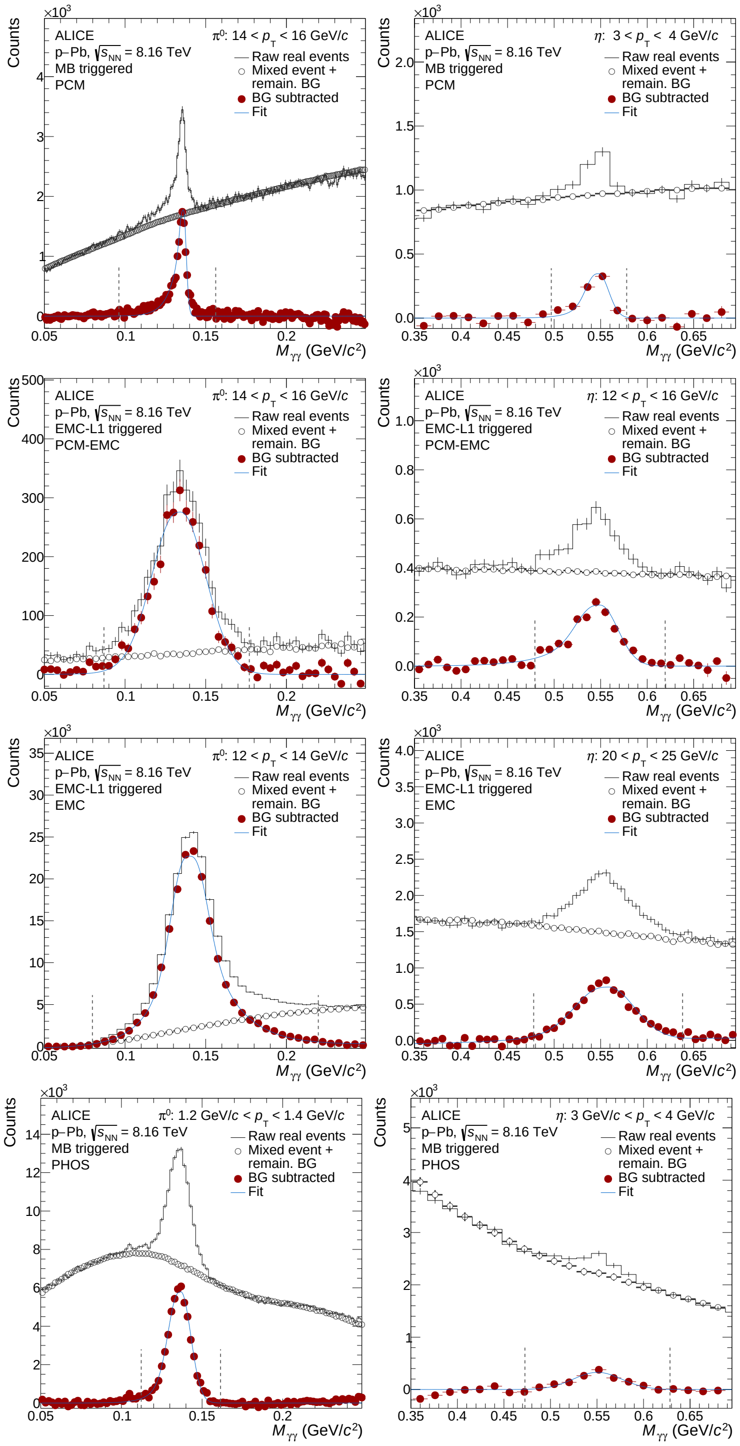

Fig. B.2: Invariant mass distributions for example transverse momentum intervals around the π^0 (left) and η (right) meson rest mass for PCM, PCM-EMC, EMC and PHOS from top to bottom. The raw invariant mass distribution is shown in black, the scaled event mixing background including an additional linear correction in gray and the signal is given by red points together with a fit function shown in blue. Integration ranges for the raw yield extraction are indicated by the vertical dashed lines.

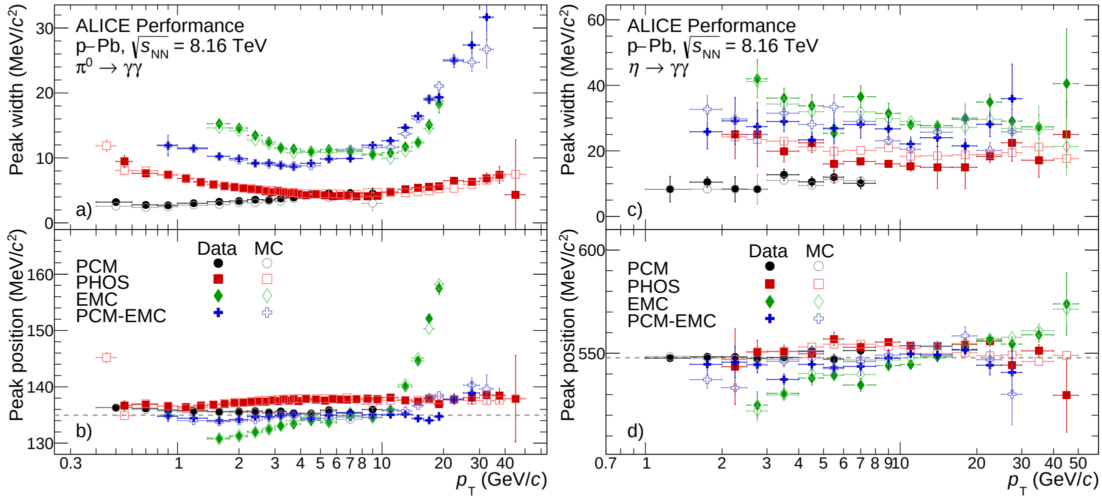

Fig. B.3: Invariant mass peak width, shown in panels a) and c), and position, shown in panels b) and d), for π^0 (left) and η (right), obtained from the fits on the invariant mass distributions, versus transverse momentum for PCM, PCM-EMC, EMC and PHOS in p–Pb collisions at $\sqrt{s_{NN}} = 8.16$ TeV. Data is presented with full markers while Monte Carlo simulation parameters are given by open markers. Vertical error bars represent statistical uncertainties. The gray dashed line in panels b) and d) indicates the respective meson rest mass.

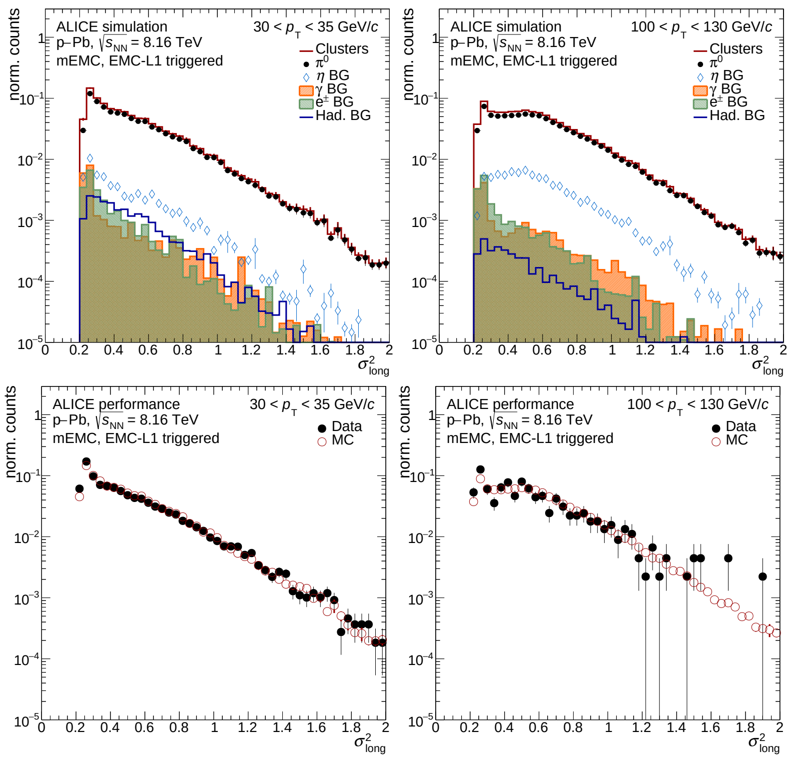

Fig. B.4: Shower shape distribution for the elongation σ^2_{long} in PYTHIA 8 Monte Carlo simulations (top) showing the various contributions to the full cluster sample for two example p_T intervals. The bottom panels show a comparison of the σ^2_{long} distributions in data and simulation in the same p_T intervals.

B.3 Total correction factors

The p_T-dependent total correction factors for the PCM, PHOS, EMC, PCM-EMC, and mEMC neutral meson reconstruction are shown in Figure B.5. They are composed of the reconstruction efficiency (ε_{rec}), the geometrical acceptance (A), the purity correction (P), and normalization factors for each reconstruction technique.

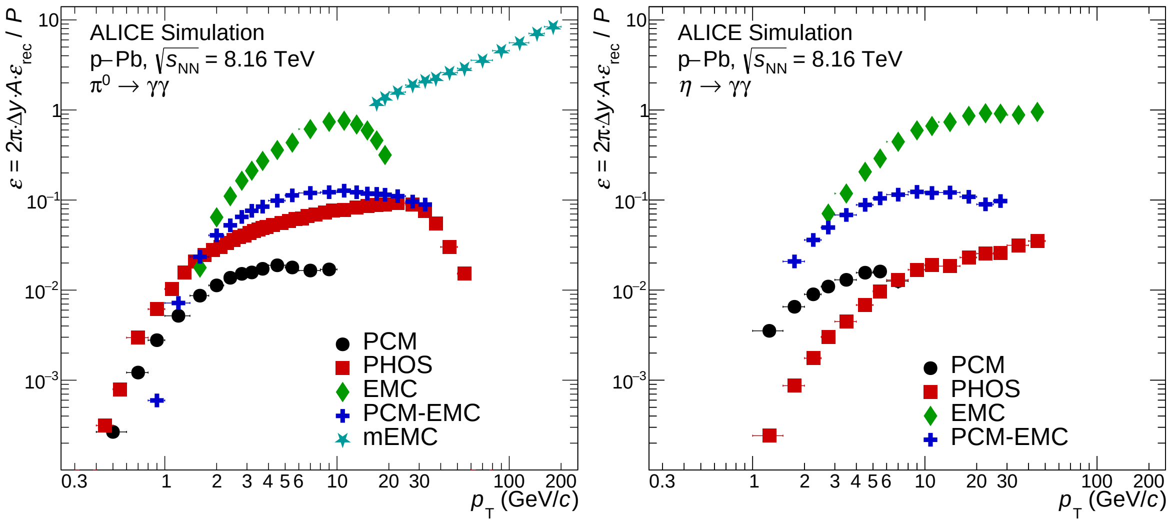

Fig. B.5: Total correction factor comprised of reconstruction efficiency ε_{rec}, kinematic acceptance A, purity P and normalization factors based on the analyzed rapidity window of each reconstruction method as a function of the meson transverse momentum.

B.4 Systematic uncertainties

An overview of the detailed systematic uncertainties for each reconstruction technique for example p_{T}-intervals is provided in Table B.2 to Table B.6 for the π^0 and η meson spectra, the η/π^0 ratio, as well as the respective nuclear modification factors. The combined statistical and systematic uncertainties according to the BLUE method [40, 41] are listed, excluding the normalization uncertainty of the minimum bias trigger cross section (σ_{MB}).

Table B.2: Summary of relative systematic uncertainties in percent for selected p_{T} intervals for the reconstruction of π^0 mesons in p–Pb collisions at $\sqrt{s_{\mathrm{NN}}} = 8.16$ TeV. The statistical uncertainties are given in addition to the total systematic uncertainties for each bin. The combined statistical and systematic uncertainties are also listed, obtained by applying the BLUE method [40, 41] for all reconstruction methods available in the given p_{T} bin, considering the uncertainty correlations for the different methods. The uncertainty from σ_{MB} determination of 1.9%, see Ref. [48], is independent of the reported measurements and is separately indicated in the figures appearing in the main body of the letter.

p_{T} interval	1.4 – 1.8 GeV/c				5 – 6 GeV/c				16 – 18 GeV/c				100 – 130 GeV/c
Method	PCM	PCM-EMC	EMC	PHOS	PCM	PCM-EMC	EMC	PHOS	PCM-EMC	EMC	PHOS	mEMC	mEMC
Signal extraction	4.1	2.4	3.5	2.1	6.9	1.0	4.1	2.9	1.5	7.3	4.9	8.3	9.5
Inner material	9.0	4.5	-	-	9.0	4.5	-	-	4.5	-	-	-	-
Outer material	-	2.8	4.2	2.0	-	2.8	4.2	2.0	2.8	4.2	2.0	2.1	2.1
PCM track rec.	0.2	0.9	-	-	0.4	0.8	-	-	0.4	-	-	-	-
PCM electron PID	0.7	0.4	-	-	0.6	0.5	-	-	0.7	-	-	-	-
PCM photon PID	0.7	0.9	-	-	1.0	2.0	-	-	2.1	-	-	-	-
Cluster description	-	1.5	5.5	1.1	-	2.0	3.6	0.1	2.9	5.2	-	3.8	4.3
Cluster energy calib.	-	1.5	1.9	2.3	-	1.5	1.9	3.1	1.5	1.9	3.2	3.3	3.3
Track match to cluster	-	0.2	0.2	-	-	0.7	0.3	-	0.5	1.1	-	-	-
Efficiency	-	1.0	2.3	1.9	-	1.0	2.3	1.9	1.0	3.0	2.0	3.6	3.6
Trigg. norm.&pileup	4.7	-	-	2.0	3.3	-	-	2.0	2.8	2.8	2.8	1.9	1.9
Total syst. uncertainty	11.0	6.4	8.3	5.5	11.9	6.5	7.6	5.2	7.4	10.9	7.0	10.7	11.9
Statistical uncertainty	2.2	2.2	3.1	1.1	6.7	3.7	2.0	3.1	3.6	4.2	3.6	2.4	5.7
Combined stat. unc.	1.0				1.8				2.2				5.7
Combined syst. unc.	3.6				3.9				4.9				11.9

Table B.3: Summary of relative systematic uncertainties in percent for selected p_{T} intervals for the reconstruction of η mesons, see Tab. B.2 for further explanations that also apply here.

p_{T} interval	2.5 – 3.0 GeV/c				6 – 8 GeV/c				20 – 25 GeV/c		
Method	PCM	PCM-EMC	EMC	PHOS	PCM	PCM-EMC	EMC	PHOS	PCM-EMC	EMC	PHOS
Signal extraction	3.8	3.3	23.7	18.0	5.0	4.7	7.3	4.5	14.4	3.0	7.0
Inner material	9.0	4.5	-	-	9.0	4.5	-	-	4.5	-	-
Outer material	-	2.8	4.2	1.8	-	2.8	4.2	1.8	2.8	4.2	1.8
PCM track rec.	1.2	1.9	-	-	2.0	2.8	-	-	1.3	-	-
PCM electron PID	1.3	4.2	-	-	3.2	1.9	-	-	2.9	-	-
PCM photon PID	2.6	3.9	-	-	4.1	4.7	-	-	6.0	-	-
Cluster description	-	3.3	5.1	2.0	-	3.6	5.9	2.0	5.2	7.5	2.0
Cluster energy calib.	-	1.5	6.7	3.1	-	1.5	4.2	3.2	1.5	3.3	3.2
Track match to cluster	-	1.4	0.8	-	-	1.6	0.9	-	2.3	2.3	-
Efficiency	-	1.0	2.3	1.6	-	1.0	2.5	1.6	1.0	2.6	1.6
Trigg. norm.&pileup	4.9	-	-	-	4.1	1.7	1.7	1.9	2.8	2.8	1.9
Total syst. uncertainty	11.4	9.6	25.6	19.1	12.4	10.3	11.6	6.8	18.0	10.7	8.5
Statistical uncertainty	12.0	14.2	20.8	29.7	25.9	11.4	7.9	6.5	16.4	6.9	15.9
Combined stat. unc.	8.6				4.5				8.2		
Combined syst. unc.	5.6				5.3				6.1		

Table B.4: Summary of relative systematic uncertainties in percent for selected p_{T} intervals for the determination of the η/π^0 ratio. The p_{T} independent systematic uncertainties associated with the material budget and the trigger normalization, as given in Tab. B.2 and Tab. B.3, are canceled in the ratio. The statistical uncertainties are given in addition to the total systematic uncertainties for each bin. The combined statistical and systematic uncertainties are also listed, see explanation in caption of Tab. B.2.

p_{T} interval	$2.5-3.0$ GeV/c				$6-8$ GeV/c				$20-25$ GeV/c		
Method	PCM	PCM-EMC	EMC	PHOS	PCM	PCM-EMC	EMC	PHOS	PCM-EMC	EMC	PHOS
Signal extraction	3.9	11.5	23.9	34.6	5.2	6.3	7.9	7.9	14.4	8.6	12.4
PCM track rec.	1.2	2.4	-	-	2.0	1.2	-	-	1.6	-	-
PCM electron PID	0.6	5.1	-	-	1.3	1.6	-	-	3.0	-	-
PCM photon PID	2.4	3.9	-	-	4.0	4.0	-	-	7.0	-	-
Cluster description	-	2.9	6.6	-	-	3.1	6.2	-	3.9	7.8	-
Cluster energy calib.	-	1.5	3.0	-	-	1.5	3.0	-	1.5	3.0	-
Track match to cluster	-	1.4	0.6	-	-	1.4	0.7	-	2.7	2.1	-
Efficiency & pileup	2.5	1.4	2.0	1.0	1.8	1.4	2.5	1.0	1.4	2.5	1.0
Total syst. uncertainty	5.6	13.9	25.1	34.7	7.2	8.7	10.8	8.0	17.2	12.4	12.5
Statistical uncertainty	12.9	14.1	20.9	17.5	25.9	14.0	8.1	5.8	16.9	12.5	12.9
Combined stat. unc.	8.6				4.5				8.2		
Combined syst. unc.	5.6				5.3				6.1		

Table B.5: Summary of relative systematic uncertainties in percent for selected p_{T} intervals for the determination of the π^0 meson nuclear modification factor R_{pPb}. The p_{T} independent systematic uncertainty associated with the material budget is canceled in the ratio. The statistical uncertainties are given in addition to the total systematic uncertainties for each bin. The combined statistical and systematic uncertainties are also listed, see explanation in caption of Tab. B.2. The uncertainties from the σ_{MB} determination in both collision systems are independent of the reported measurements and their quadratic sum of 3.4% is separately indicated in the figures appearing in the main body of the letter.

p_{T} interval	$1.4-1.8$ GeV/c				$5-6$ GeV/c				$16-18$ GeV/c				$100-130$ GeV/c
Method	PCM	PCM-EMC	EMC	PHOS	PCM	PCM-EMC	EMC	PHOS	PCM-EMC	EMC	PHOS	mEMC	mEMC
Signal extraction	2.6	2.9	5.1	3.5	6.9	1.6	4.7	3.3	2.2	7.0	5.2	1.0	1.0
PCM track rec.	0.2	0.2	-	-	0.5	0.2	-	-	1.5	-	-	-	-
PCM electron PID	0.3	0.9	-	-	0.5	0.9	-	-	1.0	-	-	-	-
PCM photon PID	0.7	0.9	-	-	1.4	1.9	-	-	2.7	-	-	-	-
Cluster description	-	1.0	4.7	0.1	-	1.5	2.5	0.1	1.8	4.1	0.1	2.0	3.1
Cluster energy calib.	-	1.5	0.8	2.0	-	1.5	0.8	2.0	1.5	0.8	2.0	1.0	1.0
Track match to cluster	-	0.2	0.2	-	-	0.4	0.3	-	2.9	1.1	-	0.5	1.5
Efficiency	-	0.5	1.7	7.3	-	0.5	1.7	7.3	0.5	1.7	7.3	0.9	0.9
Trigg. norm.&pileup	5.2	-	-	1.2	6.3	3.2	-	1.2	4.9	4.2	12.6	3.7	3.7
Total syst. uncertainty	6.5	3.7	7.2	8.9	9.5	5.7	5.6	8.7	7.3	9.3	15.6	4.6	5.4
Statistical uncertainty	3.0	2.6	4.4	5.4	9.2	5.7	3.1	6.9	5.1	5.3	11.7	2.7	10.8
Combined stat. unc.	1.8				2.7				2.2				10.8
Combined syst. unc.	2.7				2.9				2.9				5.4

Table B.6: Summary of relative systematic uncertainties in percent for selected p_T intervals for the determination of the η meson nuclear modification factor R_{pPb}. The statistical uncertainties are given in addition to the total systematic uncertainties for each bin. The combined statistical and systematic uncertainties are also listed, see explanation in caption of Tab. B.2. The uncertainty from σ_{MB} determination in both collision systems is independent of the reported measurements and is added in quadrature and separately indicated in the figures appearing in the main body of the letter.

p_T interval	2.5 – 3.0 GeV/c			6 – 8 GeV/c			20 – 25 GeV/c	
Method	PCM	PCM-EMC	EMC	PCM	PCM-EMC	EMC	PCM-EMC	EMC
Signal extraction	4.2	5.5	29.4	6.3	5.4	8.3	8.3	4.8
PCM track rec.	0.5	0.7	-	0.5	0.7	-	0.7	-
PCM electron PID	0.4	1.2	-	0.7	1.9	-	3.4	-
PCM photon PID	1.9	4.8	-	2.9	5.1	-	5.1	-
Cluster description	-	2.4	6.6	-	2.8	6.2	9.1	7.6
Cluster energy calib.	-	1.5	2.0	-	1.5	2.0	1.5	2.0
Track match to cluster	-	0.5	0.8	-	0.7	0.9	2.9	2.3
Efficiency	-	0.2	2.6	-	0.2	2.6	0.2	2.9
Trigg. norm.&pileup	6.1	-	-	6.1	3.2	-	4.9	4.2
Total syst. uncertainty	7.7	8.0	30.3	9.3	9.0	10.9	15.0	10.8
Statistical uncertainty	18.7	18.2	23.9	37.3	19.8	15.4	21.9	27.8
Combined stat. unc.	11.9			11.6			17.2	
Combined syst. unc.	5.9			6.8			11.5	

B.5 Comparison of neutral meson spectra from different reconstruction techniques

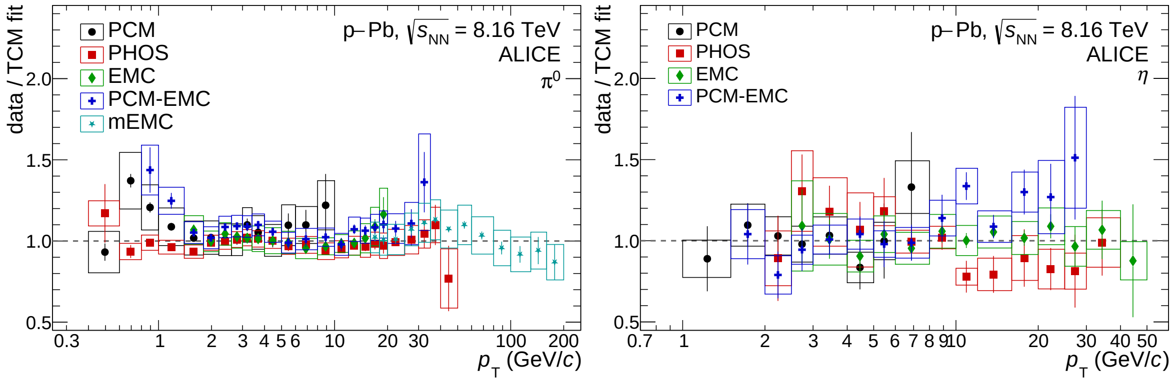

Fig. B.6: Ratio of the neutral pion (left) and η meson (right) invariant differential cross sections to the two-component model (TCM) fit of the combined spectrum for the different reconstruction techniques PCM, PCM-EMC, EMC, PHOS and mEMC in p–Pb collisions at $\sqrt{s_{NN}} = 8.16$ TeV. Statistical uncertainties are given by the vertical error bars while systematic uncertainties are shown as boxes.

B.6 Fit parameters

The combined spectra of both neutral mesons are fitted with a two-component model (TCM), proposed in Ref. [42], by using the total uncertainties for each p_T interval, which are obtained via a quadratic sum of the statistical and systematic uncertainties. The fit function is able to describe the spectra over the full p_T range and is defined as:

$$E\frac{d^3\sigma}{dp^3} = A_e \exp\left(-E_{T,kin}/T_e\right) + A\left(1+\frac{p_T^2}{T^2 n}\right)^{-n}, \tag{B.3}$$

where $E_{T,kin} = \sqrt{p_T^2 + m^2} - m$ is the transverse kinematic energy with the meson rest mass m, and A_e, A, T_e, T, and n are the free parameters. The fit parameters extracted from the TCM fit are summarized in Tab. B.7 for p–Pb and pp collisions.

Table B.7: Parameters of the fits to the π^0 and η invariant differential cross sections using the TCM fit [42] from Eq. B.3 for pp collisions at $\sqrt{s} = 8$ TeV and p–Pb collisions at $\sqrt{s_{NN}} = 8.16$ TeV.

	TCM	A_e (pb GeV$^{-2}c^3$)	T_e (GeV)	A (pb GeV$^{-2}c^3$)	T (GeV)	n	χ^2/NDF
p–Pb	π^0	$(2.47\pm1.82)\times10^{11}$	0.094 ± 0.015	$(4.38\pm0.38)\times10^{12}$	0.649 ± 0.012	3.034 ± 0.008	0.36
	η	$(2.01\pm2.82)\times10^{10}$	0.685 ± 0.183	$(4.73\pm2.69)\times10^{11}$	0.781 ± 0.095	2.917 ± 0.053	0.31
pp	π^0	$(4.98\pm2.09)\times10^{11}$	0.146 ± 0.020	$(3.73\pm0.67)\times10^{10}$	0.597 ± 0.021	3.042 ± 0.010	0.25
	η	$(0.52\pm3.24)\times10^{9}$	0.217 ± 0.211	$(2.95\pm1.10)\times10^{9}$	0.801 ± 0.069	3.012 ± 0.036	0.38

Furthermore, the region $p_T > 3.5$ GeV/c of the spectra can be fitted with a pure power-law function given by $f_{pow} = A/x^n$ in order to compare the spectral slope between different collision systems and collision energies. The fit parameters for the power-law functions on the π^0 and η meson spectra are given in Tab. B.8. The power n of the fits in pp and p–Pb show compatible values within uncertainties.

In addition, the high-p_T plateau regions of the η/π^0 ratios in pp and p–Pb collisions are fitted with constant values for $p_T > 4$ GeV/c. The values obtained from these fits are $C_{pPb}^{\eta/\pi^0} = 0.479 \pm 0.009(\text{stat}) \pm 0.010(\text{sys})$ for p–Pb collisions at $\sqrt{s_{NN}} = 8.16$ TeV and $C_{pp}^{\eta/\pi^0} = 0.473 \pm 0.006(\text{stat}) \pm 0.011(\text{sys})$ for pp collisions at $\sqrt{s} = 8$ TeV.

Table B.8: Parameters of the fits to the π^0 and η invariant differential cross sections using a pure power-law fit for pp collisions at $\sqrt{s} = 8$ TeV and p–Pb collisions at $\sqrt{s_{\mathrm{NN}}} = 8.16$ TeV.

	Power-law	A (pb GeV$^{-2}c^3$)	n	χ^2/NDF
p–Pb	π^0	(6.95±0.26)×10^{12}	5.985±0.015	0.82
	η	(2.26±0.55)×10^{12}	5.800±0.091	0.34
pp	π^0	(3.74±0.12)×10^{10}	6.006±0.015	0.90
	η	(1.38±0.15)×10^{10}	5.876±0.047	0.32